

Estudio experimental de acopladores bicónicos de fibra óptica aplicados al desarrollo de multiplexores por división de longitud de onda

M.V. Hernández-Arriaga^{a,b}, M. Bello-Jiménez^{a,*}, B. Ibarra-Escamilla^b, A. Loredó-Trejo^a,
M. Durán-Sánchez^c, H. Santiago-Hernández^b, and E.A. Kuzin^b

^aInstituto de Investigación en Comunicación Óptica, Universidad Autónoma de San Luis Potosí,
Av. Karakorum 1470 Lomas 4a Secc., 78210 San Luis Potosí, S.L.P, México.

^bInstituto Nacional de Astrofísica, Óptica y Electrónica,
L.E. Erro 1, Sta. Ma. Tonantzintla, Pue. 72824, México,

^cCONACyT- Instituto Nacional de Astrofísica, Óptica y Electrónica,
L.E. Erro 1, Sta. Ma. Tonantzintla, Pue. 72824, México,

*e-mail: m.bello@cactus.iico.uaslp.mx

Received 10 August 2017; accepted 19 September 2017

Se reporta un estudio experimental de la técnica de fabricación de acopladores bicónicos de fibra óptica y su aplicación al desarrollo de multiplexores por división de longitud de onda (WDM, wavelength division multiplexer). Los parámetros de fabricación requeridos para el WDM son obtenidos del análisis teórico de la respuesta espectral de un acoplador débilmente fusionado. Como caso particular, se reporta el desarrollo de un WDM 1550/1850 nm, el cual es un dispositivo fundamental en el desarrollo de láseres de fibra óptica dopada con Tulio. Las dimensiones finales del dispositivo son una longitud total de 36.3 mm, una cintura uniforme de 6.5 mm de largo con una sección transversal de 23 μm . El dispositivo exhibe bajas pérdidas por inserción de 0.17 dB, un espaciamiento entre canales de 303.52 nm y ancho de banda de ± 50 nm. Este trabajo establece una guía de fabricación para el desarrollo de acopladores y dispositivos WDM de fibra óptica.

Descriptores: Acopladores bicónicos de fibra; multiplexación por división de longitud de onda; laser de fibra dopada de Tulio.

An experimental study of the technique of fused biconical fiber couplers for the development of wavelength division multiplexers (WDM) is presented. The fabrication parameters required for the WDM are obtained from the theoretical analysis of the spectral response of a weakly fused coupler. As a particular case, the development of a 1550/1850 nm WDM is reported, which is a fundamental device in the implementation of Thulium-doped fiber lasers. The WDM has the total length of 36.3 mm, and a uniform tapered waist length of 6.5 mm with 23 μm of cross section. The device exhibits insertion losses of 0.17 dB, a channel spacing of 303.52 nm and a ± 50 nm bandwidth. This publication could be considered a guide for the development of fiber optic couplers and WDM devices.

Keywords: Fused fiber couplers; wavelength division multiplexing; Thulium doped fiber laser.

PACS: 07.60.Vg; 42.55.Wd; 42.81.Qb

1. Introducción

Durante las últimas décadas los dispositivos ópticos fabricados bajo la técnica de fusión y estiramiento [1] se han convertido en componentes cruciales para la implementación de sistemas ópticos. Uno de los componentes más exitosos fabricado bajo esta técnica y que se ha mantenido con un significativo interés es el acoplador bicónico, el cual ha sido extensamente analizado bajo diferentes aproximaciones [2-6]. En los últimos años, con el desarrollo de los láseres todo-fibra el acoplador se ha convertido en un dispositivo de gran demanda debido a sus aplicaciones prácticas, principalmente en la división de haces mediante canales ópticos; sin embargo, al mismo tiempo se ha optimizado su desempeño mediante procesos de fabricación de alta precisión consiguiendo reducir su tamaño y sus pérdidas de inserción. Con la introducción de nuevos medios de ganancia en las cavidades láser de fibra óptica, el acoplador debe ser objeto de constante desarrollo en su diseño con la finalidad de operar en diferentes longitudes de onda. No obstante, el alcance experimental del dispositivo contempla aplicaciones más complejas que la simple división de haces; un acoplador bicónico 2×2 (constituido

por dos puertos de entrada y dos puertos de salida) fabricado mediante un proceso debidamente controlado, produce un espectro sinusoidal de transmisión dependiente de la longitud de onda de fabricación, de tal manera que una manipulación adecuada del proceso de fabricación puede permitir que los acopladores operen en una extensa gama de aplicaciones como divisores de polarización [7,8], filtros [9,10], sensores de fibra óptica [11-13] y componentes para el multiplexado de longitudes de onda (WDM, wavelength division multiplexer) [14,15], entre otros. En el caso específico de un WDM, estos dispositivos típicamente están constituidos por un puerto de entrada y dos puertos de salida, y una de sus aplicaciones más esenciales es en cavidades láser de fibra óptica, donde los haces de bombeo y señal se multiplexan para formar una cavidad todo-fibra. Entre las características deseables para un WDM podemos mencionar un bajo costo de fabricación, bajas pérdidas de inserción y una fácil integración con componentes de fibra óptica.

En este artículo nuestro objetivo es reportar las condiciones para la fabricación de acopladores bicónicos de fibra óptica y su implementación como dispositivos WDM. El proceso de fabricación se fundamenta en un análisis de la respuesta

Abrupt-tapered fiber filter arrangement for a switchable multi-wavelength and tunable Tm-doped fiber laser

B. IBARRA-ESCAMILLA,^{1,*} M. V. HERNÁNDEZ-ARRIAGA,¹ M. DURÁN-SÁNCHEZ,² H. SANTIAGO-HERNÁNDEZ,¹ M. BELLO-JIMÉNEZ,³ E. RIVERA PÉREZ,⁴ L. A. RODRÍGUEZ-MORALES,¹ AND E. A. KUZIN¹

¹Instituto Nacional de Astrofísica, Óptica y Electrónica, Optics Department, L. E. Erro 1, Sta. Ma. Tonantzintla, Pue. 72824, Mexico

²CONACYT-Instituto Nacional de Astrofísica, Óptica y Electrónica, Optics Department, L. E. Erro 1, Sta. Ma. Tonantzintla, Pue. 72824, Mexico

³Instituto de Investigación en Comunicación Óptica, Universidad Autónoma de San Luis Potosí, Av. Karakorum 1470, Lomas 4ta Secc., San Luis Potosí, S.L.P., 78210, Mexico

⁴Departamento de Física Aplicada y Electromagnetismo-ICMUV, Universidad de Valencia, Dr. Moliner 50; Burjassot, Valencia; 46100, Spain

*baldemar@inaoep.mx

Abstract: A switchable and tunable multi-wavelength Tm-doped fiber laser is successfully demonstrated using a filter constructed with two tapered fiber elements in the cavity. The proposed system design uses a low-cost simple filter that allows stable dual, triple, quadruple, and quintuple-wavelength emission operation in the region around 1.9 μm . In the dual wavelength regime, the laser is capable of independently tuning each wavelength. For switching and tuning, a curvature is applied to the tapered fibers.

© 2018 Optical Society of America under the terms of the [OSA Open Access Publishing Agreement](#)

OCIS codes: (140.3510) Lasers, fiber; (230.7408) Wavelength filtering devices; (140.3600) Lasers, tunable.

References and links

1. S. Diaz, "Stable dual-wavelength erbium fiber ring laser with optical feedback for remote sensing," *J. Lightwave Technol.* **34**(19), 4591–4595 (2016).
2. A. Pal, S. Y. Chen, R. Sen, T. Sun, and K. T. V. Grattan, "A high-Q low threshold thulium-doped silica microsphere laser in the 2 μm wavelength region designed for gas sensing applications," *Laser Phys. Lett.* **10**(8), 085101 (2013).
3. X. L. Zhang, K. J. Zhou, N. Q. Ngo, T. H. Tan, and W. C. Poon, "Multi-wavelength fiber source with equal frequency spacing," *Laser Phys.* **20**(7), 1625–1628 (2010).
4. J. Wang, W. Zhang, L. Li, and Q. Yu, "Breath ammonia detection based on tunable fiber laser photoacoustic spectroscopy," *Appl. Phys. B* **103**(2), 263–269 (2011).
5. T. Tiess, M. Becker, M. Rothhardt, H. Bartelt, and M. Jäger, "Independently tunable dual-wavelength fiber oscillator with synchronized pulsed emission based on a theta ring cavity and a fiber Bragg grating array," *Opt. Express* **25**(22), 26393–26404 (2017).
6. M. Y. Jeon, N. Kim, J. Shin, J. S. Jeong, S. P. Han, C. W. Lee, Y. A. Leem, D. S. Yee, H. S. Chun, and K. H. Park, "Widely tunable dual-wavelength Er^{3+} -doped fiber laser for tunable continuous-wave terahertz radiation," *Opt. Express* **18**(12), 12291–12297 (2010).
7. T. Gottschall, T. Meyer, M. Baumgartl, C. Jauregui, M. Schmitt, J. Popp, J. Limpert, and A. Tunnermann, "Fiber-based light sources for biomedical applications of coherent anti-Stokes Raman scattering microscopy," *Laser Photonics Rev.* **9**(5), 435–451 (2015).
8. K. Yin, R. Zhu, B. Zhang, T. Jiang, S. Chen, and J. Hou, "Ultrahigh-brightness, spectrally-flat, short-wave infrared supercontinuum source for long-range atmospheric applications," *Opt. Express* **24**(18), 20010–20020 (2016).
9. R. J. De Young and N. P. Barnes, "Profiling atmospheric water vapor using a fiber laser lidar system," *Appl. Opt.* **49**(4), 562–567 (2010).
10. A. Ghosh, A. S. Roy, S. D. Chowdhury, R. Sen, and A. Pal, "All-fiber tunable ring laser source near 2 μm designed for CO_2 sensing," *Sens. Actuators B Chem.* **235**, 547–553 (2016).
11. K. Bremer, A. Pal, S. Yao, E. Lewis, R. Sen, T. Sun, and K. T. V. Grattan, "Sensitive detection of CO_2 implementing tunable thulium-doped all-fiber laser," *Appl. Opt.* **52**(17), 3957–3963 (2013).

All-fiber laser with simultaneous Tm^{3+} passive Q-switched and Ho^{3+} gain-switched operation

BALDEMAR IBARRA-ESCAMILLA,¹  MANUEL DURÁN-SÁNCHEZ,^{2,*} RICARDO I. ÁLVAREZ-TAMAYO,³
BERENICE POSADA-RAMÍREZ,¹ PATRICIA PRIETO-CORTÉS,⁴ JARED ALANIZ-BAYLÓN,¹
HÉCTOR SANTIAGO-HERNÁNDEZ,¹ MIGUEL BELLO-JIMÉNEZ,⁵  AND EVGENY A. KUZIN¹

¹Instituto Nacional de Astrofísica, Óptica y Electrónica, Luis Enrique Erro, Sta. María Tonantzintla, Puebla 72824, Mexico

²CONACyT—Instituto Nacional de Astrofísica, Óptica y Electrónica, Luis Enrique Erro, Sta. María Tonantzintla, Puebla 72824, Mexico

³CONACyT—Universidad Autónoma de Nuevo León, Av. Universidad S/N, San Nicolás de los Garza, N. L. 66451, Mexico

⁴Universidad Autónoma de Nuevo León, Av. Universidad S/N, San Nicolás de los Garza, N. L. 66451, Mexico

⁵Instituto de Investigación en Comunicación Óptica, Universidad Autónoma de San Luis Potosí, Av. Karakorum 1470, S. L.P. 78210, Mexico

*Corresponding author: manued@inaoep.mx

Received 4 May 2018; revised 15 June 2018; accepted 16 June 2018; posted 18 June 2018 (Doc. ID 330968); published 11 July 2018

We experimentally demonstrate simultaneous Tm^{3+} passive Q-switched (PQS) and Ho^{3+} gain-switched laser operations at 1888.8 and 2021.2 nm, respectively, in a single-cavity all-fiber laser. The PQS operation of the Tm^{3+} laser is based on the use of a high-concentration holmium-doped fiber as a fiber saturable absorber. Then the Tm^{3+} laser emission is used as a pulsed pump source to achieve Ho^{3+} gain-switched pulses. A high birefringence fiber optical loop mirror used as a spectral filter allows the tuning of both Tm^{3+} and Ho^{3+} laser emissions. © 2018 Optical Society of America

OCIS codes: (140.3510) Lasers, fiber; (140.3070) Infrared and far-infrared lasers; (140.3538) Lasers, pulsed; (230.7408) Wavelength filtering devices; (140.5560) Pumping.

<https://doi.org/10.1364/OL.43.003377>

Pulsed thulium-doped fiber (TDF) and holmium-doped fiber (HDF) lasers operating at wavelengths around 2 μm are of persistent interest because of a wide range of applications such as spectroscopy [1], light detection and ranging [2], laser surgery in medical treatment [3], and material processing [4]. The HDF lasers allow extension of the emission wavelength range to 2.1 μm , beyond the range reached by TDF lasers [5,6]. The TDF and HDF lasers offer advantages such as high reliability, compactness, maintenance-free operation, and robustness.

Q-switched fiber lasers generate high-energy pulses with duration in the nanosecond range. Particularly, passive Q-switched (PQS) lasers based on the use of a fiber saturable absorber (FSA) are simple and cost-effective devices. The FSA is commonly an unpumped segment of a rare-earth-doped fiber, where light absorption decreases with the increasing of the light intensity. The FSA is more effective when fibers with higher dopant concentrations and short lengths are used [7]. Different approaches of PQS lasers based on fibers doped with Tm^{3+} or Ho^{3+} used as FSAs have been reported [8–11].

Another reliable alternative for pulsed generation of fiber lasers is gain-switching (GS). In this technique, pulses with nanosecond duration are generated by using a pulsed pump source, without additional components [12]. In GS lasers, the pump source directly modulates the population inversion in the energy levels of the gain medium [13]. The HDF laser generation can be achieved with pump sources at wavelengths around 1950 nm [14], which can be easily generated by TDF lasers. Therefore, TDF lasers became reliable pump sources for HDF lasers. To the best of our knowledge, only three GS HDF lasers pumped by a pulsed TDF laser source have been reported in order to obtain pulsed laser generation at the 2.1 μm wavelength range [14–16]. In the cascaded laser configurations reported in Refs. [14] and [15], the HDF was pumped by the GS TDF laser which, in turn, was pumped by the 1.55 μm pulsed fiber laser. In Ref. [16] the HDF laser was pumped by the commercial Q-switched TDF laser. The fiber optical loop mirror (FOLM) with the high birefringence (Hi-Bi) fiber loop was shown to be the reliable spectral filter to achieve tunable single and dual-wavelength operations of fiber lasers [17,18]. The longest wavelength achieved in the TDF laser using the Hi-Bi FOLM was 1970 nm [18].

In this Letter, we experimentally demonstrate simultaneous Tm^{3+} PQS and Ho^{3+} GS laser operation of a single linear cavity fiber laser. The TDF is pumped by a continuous wave (CW) laser at 1567 nm. The segment of the high-concentration HDF acts as the FSA allowing PQS operation of the TDF laser. Then the pulses generated by the TDF laser are used as the pump for the same HDF, causing GS operation of the HDF laser. The Hi-Bi FOLM is used as the spectral filter for the tuning of both generated laser wavelengths.

The experimental setup of the proposed laser is shown in Fig. 1. The linear cavity consists of the 9 m long TDF (CorActive SCF-TM-8/125) which is pumped by A double-clad Er/Yb fiber laser at 1567 nm through a 1550/2000 nm wavelength division multiplexer. An optical isolator was used to avoid damage of the pump source. A 1 m long

Letter

Actively mode-locked all-fiber laser by 5 MHz transmittance modulation of an acousto-optic tunable bandpass filter

M Bello-Jiménez¹, E Hernández-Escobar¹, A Camarillo-Avilés¹, O Pottiez²,
A Díez³ and M V Andrés³

¹ Instituto de Investigación en Comunicación Óptica (IICO), Universidad Autónoma de San Luis Potosí, Av. Karakorum No. 1470 Lomas 4ª Secc., 78210 San Luis Potosí, Mexico

² Centro de Investigaciones en Óptica (CIO), Loma del Bosque No. 115, Col. Lomas del Campestre, León, Guanajuato 37150, Mexico

³ Departamento de Física Aplicada y Electromagnetismo, Universidad de Valencia, ICMUV, c/Dr. Moliner 50, Burjassot, 46100 Valencia, Spain

E-mail: miguel.bello@uaslp.mx

Received 29 January 2018, revised 1 June 2018

Accepted for publication 2 June 2018

Published 29 June 2018



Abstract

Active mode-locking of an all-fiber ring laser by transmittance modulation of an in-fiber acousto-optic tunable bandpass filter (AOTBF) is reported. Cavity loss modulation is achieved by full acousto-optic mode re-coupling cycle induced by standing flexural acoustic waves. The modulator permits the implementation of 28 dB of nonresonant light suppression, 1.4 nm of modulation bandwidth, 74% of modulation depth and 4.11 dB of optical loss in a 72.5 cm-long all-fiber configuration. The effects of the modulated AOTBF on the laser performance are investigated. Transform-limited optical pulses of 8.8 ps temporal width and 6.0 W peak power were obtained at 4.87 MHz repetition rate.

Keywords: mode-locked fiber lasers, acousto-optic modulation, fibre optics

(Some figures may appear in colour only in the online journal)

1. Introduction

Ultrashort optical pulses with temporal widths from a few picoseconds to several hundreds of femtoseconds have become essential for a large variety of applications. Examples of these applications can be found in optical communications, biomedical research, spectroscopy and material processing, among others [1, 2]. In many of these applications the quality of the pulse is an important factor, and the generation of clean ultrashort optical pulses has attracted the attention of researchers for a relatively long time. For applications in the ultrashort pulse regime, passive mode locking is the preferable technique, but sometimes the generation of low-intensity radiation and the limited repetition rate becomes its major

shortcoming. Conversely, active mode locking allows a tight control over intracavity parameters, such as the cavity losses or the round-trip phase change, enabling improvements on the output pulse characteristics. Therefore, active mode locking is the preferred technique in many practical applications. Nevertheless, a detrimental factor of this technique is the relatively long pulse duration as a result of the limited optical bandwidth of the active mode locker.

In the framework of actively mode-locked lasers, many researchers have proposed and demonstrated different configurations to produce high-quality ultrashort optical pulses [3–9]. Among them, all-fiber arrangements are very attractive devices since they can reduce intracavity losses associated with bulk components and can be designed to adjust cavity

Numerical study of multiple noise-like pulsing in a dispersion-managed figure-eight fibre laser

O Pottiez¹, Y E Bracamontes-Rodriguez¹, H E Ibarra-Villalon^{1,2},
J C Hernandez-Garcia^{3,4}, M Bello-Jimenez⁵, J P Lauterio-Cruz³,
E Garcia-Sanchez¹ and E A Kuzin⁶

¹ Centro de Investigaciones en Óptica (CIO), Loma del Bosque 115, Col. Lomas del Campestre, León, Gto. 37150, Mexico

² Departamento de Física, Universidad Autónoma Metropolitana Iztapalapa, San Rafael Atlixco 186, Del. Iztapalapa 09340, Mexico

³ Departamento de Electrónica, División de Ingenierías CIS, Universidad de Guanajuato, Carretera Salamanca-Valle de Santiago Km 3.5+1.8 Km, Comunidad de Palo Blanco, Salamanca, Gto. 36885, Mexico

⁴ Consejo Nacional de Ciencia y Tecnología, Av. Insurgentes Sur No. 1582, Col. Crédito Constructor, Del. Benito Juárez 03940, Mexico

⁵ Instituto de Investigación en Comunicación Óptica, Universidad Autónoma de San Luis Potosí, Av. Karakorum 1470, Lomas 4ta Secc., San Luis Potosí, S.L.P. 78210, Mexico

⁶ Instituto Nacional de Astrofísica, Óptica y Electrónica (INAOE), L. E. Erro 1, Sta. Ma. Tonantzintla, Pue. 72824, Mexico

E-mail: pottiez@cio.mx

Received 9 January 2018

Accepted for publication 23 May 2018

Published 27 June 2018



CrossMark

Abstract

We study numerically noise-like pulsing in a long passively mode-locked figure-eight fibre laser with a polarization-imbalanced nonlinear optical loop mirror (NOLM) and a strong dispersion map. Contrary to the common scenario where a single noise-like pulse develops, it is found that multiple small bunches tend to form in the cavity, sharing roughly the same characteristics, which are determined by the dispersion parameters. The wave packets are subject to ample periodic variations of their duration and peak intensity as they pass through sections of opposite dispersion signs, displaying a breathing dynamics analogous to the one undergone by solitons in stretched-pulse fibre lasers. Multiple noise-like pulsing operation can be understood by considering the strong compression and corresponding intensity increase of small bunches as they travel through the NOLM, which yields higher transmission through the NOLM and thus smaller cavity losses for these small units than for larger wave packets. The present results could serve as a basis for a deeper study of the dynamics taking place in partially mode-locked fibre sources, which is particularly complex when multiple bunches of radiation coexist and interact in the cavity.

Keywords: fibre lasers, passive mode locking, noise-like pulses

(Some figures may appear in colour only in the online journal)

1. Introduction

Passively mode-locked fibre lasers (PML-FLs) are versatile sources that have received widespread recognition mainly due

to their ability to produce stable trains of solitons. In these systems, however, the complex interaction of multiple dispersive, nonlinear and dissipative effects does not always lead to stationary modes of operation, but may also give rise to a

Dissipative Soliton Resonance in a Thulium-Doped All-Fiber Laser Operating at Large Anomalous Dispersion Regime

Baldemar Ibarra-Escamilla,¹ Manuel Durán-Sánchez^{1,2},
Berenice Posada-Ramírez¹, Héctor Santiago-Hernández,³
Ricardo Iván Álvarez-Tamayo^{1,4}, David Sánchez de la Llave,¹
Miguel Bello-Jiménez,⁵ and Evgeny A. Kuzin¹

¹Instituto Nacional de Astrofísica, Óptica y Electrónica, Puebla 72824, Mexico

²CONACyT—Instituto Nacional de Astrofísica, Óptica y Electrónica, Puebla 72824, Mexico

³Departamento de Electrónica, Universidad de Guadalajara, Guadalajara 44840, Mexico

⁴CONACyT—Universidad Autónoma de Nuevo León, Nuevo León 66451, Mexico

⁵Instituto de Investigación en Comunicación Óptica, Universidad Autónoma de San Luis Potosí, San Luis Potosí 78210, Mexico

DOI:10.1109/JPHOT.2018.2870572

1943-0655 © 2018 IEEE. Translations and content mining are permitted for academic research only.

Personal use is also permitted, but republication/redistribution requires IEEE permission.

See http://www.ieee.org/publications_standards/publications/rights/index.html for more information.

Manuscript received July 6, 2018; revised September 5, 2018; accepted September 12, 2018. Date of publication September 17, 2018; date of current version October 4, 2018. This work was supported by CONACyT project 256401. Corresponding author: M. Durán-Sánchez (e-mail: manuel@inaoep.mx).

Abstract: We experimentally demonstrate dissipative soliton resonance effect in a 173-m long passively mode-locked figure-eight thulium doped fiber laser with a net anomalous dispersion. The duration of the wave-breaking-free pulse broadens with the increase of a pump power. At maximum pump power of 4.5 W, square pulses were generated with duration of 85.18 ns, average output power of 245 mW, pulse energy of 206 nJ, and repetition rate of 1.19 MHz.

Index Terms: Fiber laser, mode-locked lasers, pulse propagation, temporal solitons.

1. Introduction

Mode-locked thulium-doped fiber lasers (TDFLs) in the 2- μm wavelength band have been the subject of increasing interest for a wide range of applications in different research areas, such as microscopy [1], fiber amplifiers [2], nonlinear frequency conversion for mid-IR and THz generation [3], welding of polymeric materials [4], gas detection and analysis [5], among others. Passively mode-locked fiber lasers are considered very useful optical sources to generate stable and coherent ultrashort optical pulses. In TDFLs the generation of conventional solitons [6], [7], dissipative solitons [8], [9], and also the effect of the dissipative soliton resonance (DSR) [1], [2], [10]–[13] were demonstrated. Besides this, some quasi-stable dynamics such as the noise-like pulse (NLP) regime have been also reported [14], [15]. Several mode-locking mechanisms which include semiconductor saturable absorber mirror (SESAM) [8], [16], carbon nanotubes (CNTs) [17], graphene [7], [18], nonlinear polarization evolution (NPE) [14], [19], [20], nonlinear optical loop mirror (NOLM) [2], [14], and even combinations of them have been reported to perform a stable train of mode-locked optical pulses [21]. Saturable absorbers (SA) based on a nonlinear optical effect have the response time of around 5 fs. With combination of a nonlinear amplified fiber loop mirror (NALM) with a CNT SA,

Passively Q-Switched Thulium-Doped Fiber Laser Using Alcohol

Baldemar Ibarra-Escamilla, Manuel Durán-Sánchez^{ID}, Berenice Posada-Ramírez, Ricardo I. Álvarez-Tamayo^{ID}, Jared Alaniz-Baylón, Miguel Bello-Jiménez^{ID}, Patricia Prieto-Cortés, and Evgeny A. Kuzin

Abstract—A passively Q-switched thulium-doped fiber laser using isopropyl alcohol as a saturable absorber is experimentally demonstrated. The absorber was made of two FC/PC connectors matched into a cannula with the gap between them filled by isopropyl alcohol. The alcohol-based saturable absorber incorporated into a ring cavity thulium-doped fiber laser leads to passive Q-switching laser operation at the wavelength of 1.88 μm . With the maximum pump power of 1.42 W, passive Q-switched pulses with a minimum duration of 1.46 μs , maximum repetition rate of 66.7 kHz, and pulse energy of 0.93 μJ were obtained.

Index Terms—Fiber lasers, Q-switched lasers, saturable absorber.

I. INTRODUCTION

PASSIVELY Q-switched thulium-doped fiber lasers (TDFL) have been of persistent interest in order to generate short high-energy pulses near the 2- μm wavelength range due to their applications in light detection and ranging (LIDAR), medicine, spectroscopy, optical signal processing, and optical instrumentation. Passive Q-switched (PQS) fiber lasers exhibit attractive advantages such as compactness, simplicity, and flexibility of design. Particularly, PQS TDFL has been increasingly investigated as 2 μm compatible fiber components become readily accessible. Passive Q-switching techniques are based on the use of a saturable absorber (SA) within the laser cavity in order to vary the quality factor. In recent years, different SA including a semiconductor saturable absorber mirror (SESAM) [1]–[3], graphene [4]–[12], carbon nanotubes (CNT) [13]–[18], rare-earth-doped fibers [19], [20], and a topological insulators (TI) [21], [22],

have been proposed for PQS in fiber lasers at the 2- μm wavelength range. Recently, some transitional metal dichalcogenides (TMD) have been demonstrated as promising SA materials for lasers pulses generation [23], [24]. TMD materials such as film-type rhenium disulfide (ReS_2)-polyvinyl alcohol and tungsten disulfide (WS_2) have been included in fiber laser cavities to generate Q-switching and mode-locking pulses. SESAM has drawbacks that include narrow tuning ranges of a few tens of nanometers, high cost of fabrication, and difficult to incorporate into a fiber laser resonator. SA based on graphene and CNT composites exhibit risk of damage when used in high power fiber lasers in which PQS pulses energy reaches hundreds of nano-Joules. Rare-earth-doped fiber SAs have been introduced as a reliable alternative because they could offer fiber compatibility and simplicity, however, the flexibility of the PQS pulses characteristics are difficult to vary as they depend on the doped-fiber fabrication process. Recently, alcohol-based SAs have been introduced as an alternative to obtain passive Q-switched and mode-locking operation in erbium-doped fiber (EDF) lasers at the 1.5 μm wavelength range [25], [26]. Because of the stretching vibration and flexural vibrations of carbon hydrogen (C–H), carbon–oxygen (C–O) and oxygen hydrogen (O–H) bonds, some alcohol composites exhibits broadband absorption which spans over the wavelength range from 1.5 to 2.1 μm [26]. This feature, make them attractive as SA elements for design of pulsed fiber lasers based on EDF and TDF.

In this letter, we experimentally demonstrate Q-switched pulses generation of a ring cavity TDF laser operating near to the 2 μm wavelength region by using a liquid alcohol-based SA. PQS laser operation at the wavelength of 1.88 μm is achieved by filling with isopropyl alcohol the gap between the end-facets of two FC/PC connectors matched with a cannula. At the maximum pump power of 1.42 W the minimum pulse duration was $\sim 1.46 \mu\text{s}$ at maximum repetition rate of 66.71 kHz, with pulse peak power of 634 mW, and pulse energy of 0.93 μJ .

II. EXPERIMENTAL SETUP

Fig. 1 shows the TDFL configuration. The schematic of the alcohol-based SA is also shown. The ring cavity consists of 4-m of TDF (Coractive SCF-TM-8/125) pumped by a home-made single-mode ring cavity Er/Yb (Nufern SM-EYDC-6/125-HE) laser source, maximum power of 3.5 W at 1567 nm through a 1550/2000 nm wavelength division

Manuscript received August 20, 2018; revised August 31, 2018; accepted September 2, 2018. Date of publication September 6, 2018; date of current version September 21, 2018. This work was supported by the CONACyT Project under Grant 256401. (Corresponding author: Manuel Durán-Sánchez.)

B. Ibarra-Escamilla, B. Posada-Ramírez, J. Alaniz-Baylón, and E. A. Kuzin are with the Optics Department, Instituto Nacional de Astrofísica, Óptica y Electrónica, San Andrés Cholula 72824, Mexico (e-mail: baldemar@inaoep.mx; b.posada@inaoep.mx; jared.alaniz@inaoep.mx; ekuz@inaoep.mx).

M. Durán-Sánchez is with CONACyT, Optics Department, Instituto Nacional de Astrofísica, Óptica y Electrónica, San Andrés Cholula 72824, Mexico (e-mail: manuedl@inaoep.mx).

R. I. Álvarez-Tamayo is with CONACyT, Universidad Autónoma de Nuevo León, San Nicolás de los Garza 66451, México (e-mail: rialvarez@conacyt.mx).

M. Bello-Jiménez is with the Instituto de Investigación en Comunicación Óptica, Universidad Autónoma de San Luis Potosí, San Luis Potosí 78210, Mexico (e-mail: m.bello@cactus.iico.uaslp.mx).

P. Prieto-Cortés is with the Universidad Autónoma de Nuevo León, San Nicolás de los Garza 66451, México (e-mail: pattyprieto@hotmail.com).



Color versions of one or more of the figures in this letter are available online at <http://ieeexplore.ieee.org>.

Digital Object Identifier 10.1109/LPT.2018.2868923

Raman spectroscopy mapping of Si (001) surface strain induced by Ni patterned micro arrays

Cite as: J. Appl. Phys. **122**, 125703 (2017); <https://doi.org/10.1063/1.4985817>

Submitted: 31 May 2017 . Accepted: 18 September 2017 . Published Online: 28 September 2017

F. J. Rodríguez-Aranda, J. Méndez-Lozoya, F. J. González , and A. G. Rodríguez 



View Online



Export Citation



CrossMark

ARTICLES YOU MAY BE INTERESTED IN

[Deviations from Vegard's law in semiconductor thin films measured with X-ray diffraction and Rutherford backscattering: The \$\text{Ge}_{1-y}\text{Sn}_y\$ and \$\text{Ge}_{1-x}\text{Si}_x\$ cases](#)

Journal of Applied Physics **122**, 125702 (2017); <https://doi.org/10.1063/1.4996306>

[Investigation of optical transitions in a SiGeSn/GeSn/SiGeSn single quantum well structure](#)

Journal of Applied Physics **122**, 123102 (2017); <https://doi.org/10.1063/1.4986341>

[High photoresponsivity from multilayer \$\text{MoS}_2/\text{Si}\$ heterojunction diodes formed by vertically stacking](#)

Journal of Applied Physics **122**, 124505 (2017); <https://doi.org/10.1063/1.4994740>

Lock-in Amplifiers
up to 600 MHz



Rapid Reflectance-Anisotropy Spectroscopy as an Optical Probe for Real-Time Monitoring of Thin Film Deposition

J. Ortega-Gallegos^{1,a)}, L. E. Guevara-Macías¹, A. Lastras-Martínez¹, D. Ariza-Flores², R.E. Balderas-Navarro¹ and L.F. Lastras-Martínez¹

¹*Instituto de Investigación en Comunicación Óptica, Universidad Autónoma de San Luis Potosí, Alvaro Obregón 64, San Luis Potosí, SLP 78000, México Phone: 52 (444) 825 0183, Fax: 52 (444) 825 0198.*

²*Cátedras Conacyt, Av. Insurgentes 1582, Crédito Constructor, Delegación Benito Juárez, CDMX 03940, México.*

^{a)}Corresponding author: jortega@cactus.iico.uaslp.mx

Abstract. We report on real-time spectroscopic reflectance anisotropy measurements carried out during the epitaxial growth of GaAs/GaAs (001). Our work is aimed to the study of fundamental processes occurring during the epitaxial growth of III-V semiconductors. We show that during growth there is an oscillation in the surface strain associated to surface reconstruction, suggesting the existence of a mechanism of periodic build up-relaxation of the surface strain, indicating that the technique employed in this work may potentially distinguish between two reconstruction phases.

INTRODUCTION

The growth of well controlled surface templates with III-V epitaxy remains a challenge and is a very interesting topic due to their potential applications for nanoscale devices based on GaAs [1, 2]. For this purpose, non-invasive diagnostic probes such as Reflectance-Anisotropy Spectroscopy (RAS) would be of great value. The use of this probe in a feedback control loop would allow for the precise control of surface reconstruction during the for molecular beam epitaxy (MBE) growth. In this regards, it is known that there is close relationship between RAS line shape and surface reconstruction. In the case of the GaAs(001) surface, RAS has proved to be highly sensitive to surface reconstruction, giving information on three types of As-stabilized reconstructions, namely $\alpha(2 \times 4)$, $\beta(2 \times 4)$ and $\gamma(2 \times 4)$ [3], and $\alpha c(4 \times 4)$ and $\beta c(4 \times 4)$ [4]. It has been reported that RA spectra around E_1 and $E_1 + \Delta_1$ transitions comprise several components. Among them, we include components induced by surface roughness [5] and surface anisotropic strain fields for both $c(4 \times 4)$ [6] and (2×4) surface reconstructions [7]. Such strains are related to a surface stress arising from charge redistribution in the surface bonds due to the absence of atoms above the surface [8]. Reconstruction-induced strain has an orthorhombic symmetry and may penetrates into a region 20 nm thick [6].

Recently, we have shown that it is possible to use real-time RA spectroscopy for monitoring processes taking place during the homoepitaxial growth of GaAs/GaAs (001) [9]. In this paper we report on a real-time RAS investigation of the dynamics of homoepitaxial MBE growth of GaAs (001) at a temperature of 520 °C. Particularly, we focus on the study of RA amplitude oscillations that are linked to the layer by layer growth model. We note that the growth temperature employed in this work is one of the standards in the manufacture of thin films for optoelectronic device applications.

EXPERIMENTAL DETAILS

Undoped GaAs films were grown on GaAs (001) substrates in a solid source molecular beam epitaxy system (Riber 32P). A home made rapid RA spectrometer attached to the growth chamber enables the acquisition of RA spectra at a rate of 10 spectra/s [10]. The setup allows for the simultaneous measurement of RA spectra and Reflection High Energy Electron Diffraction (RHEED) oscillations during growth. To remove the surface native oxide the GaAs substrate was heated to at a temperature 600 °C until a (2×4) RHEED pattern was observed. An undoped 0.3 μm thick buffer

Real-time Optical Monitoring of Semiconductor Epitaxial Growth

A. Lastras-Martínez^{1,a)}, J. Ortega-Gallegos¹, L.E. Guevara-Macías¹, D. Ariza-Flores², O. Núñez-Olvera¹, R.E. López-Estopier², R.E. Balderas-Navarro¹ and L.F. Lastras-Martínez¹

¹ *Instituto de Investigación en Comunicación Óptica, Universidad Autónoma de San Luis Potosí, San Luis Potosí, México.*

² *Cátedras Conacyt, Av. Insurgentes 1582, Crédito Constructor, Delegación Benito Juárez, CDMX 03940, México.*

^{a)}Corresponding author: alastras@gmail.com

Abstract. We report on time-resolved Reflectance Anisotropy Spectroscopy (RAS) measurements carried out during the molecular beam epitaxial growth of GaAs (001). Growth started on a c(4x4) reconstructed surface which changed to (2x4) and then to (4x) as growth progressed. We found that reflectance anisotropy spectra comprise three components, each one with a specific physical origin and determine their time evolution as a function of epitaxil film thickness. We conclude that RAS is a powerful probe for the monitoring and potentially for the control of epitaxial growth.

INTRODUCTION

Light probes, being non-invasive, result very attractive tools for the real-time monitoring of the epitaxial growth of semiconductors. Depending on photon energy, however, light impinging on the substrate penetrates to a depth of 50-500 monolayer, thus limiting surface sensitivity. More than two decades ago, D.E. Aspnes introduced Reflectance-anisotropy spectroscopy (RAS) (also known as Reflectance-difference spectroscopy) which overcomes this limitation by measuring the difference in reflectivity for two mutually orthogonal polarizations [1]. In the past, however, despite the demonstrated RAS surface sensitivity, its use for epitaxial growth monitoring has been hindered by 1) the lack of reflectance anisotropy (RA) spectrometers fast enough to follow atomic processes during growth and 2) the limited understanding of the physics underlining the optical anisotropy of semiconductor surfaces. Here we address these two points and report on time-resolved RAS measurements carried out during the MBE homoepitaxial growth of GaAs (001) that show RAS to be a powerful probe for the monitoring and control of epitaxial growth.

EXPERIMENTAL

Epitaxial growth was carried out on GaAs (001) substrates in a solid source molecular beam epitaxy chamber (Riber 32P). Growth temperature and As₄ overpressure were set to 520 °C and 2x10⁻⁶ Torr, respectively. With these conditions, during the first growth stage the GaAs film growth rate was 0.19 ML/s, decreasing to 0.13 ML/s as growth stabilized. Prior to RA measurements a 0.2 μm thick undoped GaAs buffer layer was grown on the GaAs substrate. The sample surface is kept under As₄ flux along the whole experiment. Growth is started upon opening the Ga shutter on a c(4x4) reconstructed surface which first changes to (2x4) and then to a Ga-rich reconstruction. As discussed below, the RA spectrum line shape changes substantially along growth.

Comparative Study of CdS and CdS/ZnS Thin Films Deposited by CBD as a Buffer Layer Solar Cell

A. García-Barrientos¹, H. Gomez-Pozos², E. Villicaña-Ortiz³ and L. Cruz-Netro⁴

¹. Faculty of Science, Universidad Autónoma de San Luis Potosí, SLP, México.

². Electronics Department, Universidad Autónoma del Estado de Hidalgo, Hidalgo, México.

³. Departamento de Ingeniería de la Energía, Universidad de Ingeniería y Tecnología, Lima, Peru

⁴. Ingeniería Industrial, Universidad Politécnica de Altamira, México

Cadmium sulphide (CdS) and Cadmium sulphide/Zinc sulfide (CdS/ZnS) thin films have been extensively investigated as an *n*-type buffer layer to form thin film heterojunction solar cells with *p*-CdTe absorber layers. The buffer layer affects the electrical properties of the junction and protects it from chemical reactions. From the electronic point of view, the CdS and CdS/ZnS layers can optimize the band alignment of the device [1 and 2]. Also, these can build a sufficiently wide depletion width that minimizes tunneling and establishes a higher contact potential that allows higher open circuit voltage [2]. Recently, a particular attention of the researches has been focused on the heterostructures involving CdS and CdS/ZnS multilayers [3]. Because of its band gap, it could be an excellent window layer in CdTe thin film solar cells. Since Chemical Bath Deposition (CBD) is known to produce solar cells over a large area at a low cost and low temperature. The effect of deposition parameters of CdS and CdS/ZnS thin films developed by CBD technique were investigated in [4 and 5], principally, the influence of pH control of the reaction solution on the structural and optical properties of chemically deposited CdS and CdS/ZnS thin films. Different films thicknesses of CdS and CdS/ZnS thin films were deposited onto a glass substrate. The structural surface morphology of as-deposited CdS and CdS/ZnS thin films was characterized by SEM. The physical conditions were kept identical while growing of the samples. The investigation of the effect of the synthesis method on the change the ammonium hydroxide by buffer pH (from 10.1 - 13) contributed in increases the growth kinetics, resulting in thicker films.

In this paper, a comparative study of CdS and CdS/ZnS thin films deposited by CBD as a buffer layer solar cell was carried out. The CdS and CdS/ZnS thin films were fabricated by CBD technique on a glass substrate for a deposition time of 60 minutes at a bath temperature of 90 °C. These thin films were synthesized by chemical bath deposition using acid as a complexing agent with pH values between 10.1 to 11.3 for the CdS thin films and for the CdS/ZnS thin films with pH values between 11.4 to 13, these can be seen in the Figures 1a and 1b, respectively. The SEM photos (see figure 1a) show the surfaces of CdS films grown at 60 minutes deposition time and to different solution pH values. Based on the optical transmission measurements, the square of absorption coefficient (α^2) is plotted as a function of photon energy ($h\nu$) in figure 1c, one can see the energy band gap, E_g , values 2.38, 2.58 and 2.44 eV for pH values, 10.1, 10.6 and 11.3, respectively. In the other case, for the CdS/ZnS thin films grown at 60 minutes time deposition, one can see the SEM photos of the samples surfaces in the figure 1c. Also, we found different energy band gaps for different pH values; for pH=11.4, E_g equals 2.74 eV and at pH=11.8, E_g equals 2.7 eV, these values are pretty similar of the literature [6]. Finally, these studies show that the pH contributes noticeably to the growth and to the structure of deposited CdS and CdS/ZnS multilayer films. This may be interpreted by the decrease of the film thickness. From these studies, we are able to optimize the process in order to produce the layer suitable for optical window in solar cells. For the case of CdS thin films, it is better to use acid as a complexing agent with pH value equal to 10.6 and for the case of CdS/ZnS thin films, it is better use with pH value equal to 11.4. This approach could be used in improving the spectral response of CdTe-based solar cells. A higher band gap was observed for CdS/ZnS, it indicates that there is clear short-wavelength advantages in current

Infrared Ellipsometry Analysis of Heritage Photographic Prints

A. Nieto-Villena¹, J. R. Martínez², J. M. Flores-Camacho³, A. Lastras-Martínez³, J. A. de la Cruz-Mendoza⁴, G. Ortega-Zarzosa², J. C. Valcárcel-Andrés⁵ and Á. Solbes-García¹

¹Facultad del Hábitat, Benemérita Universidad Autónoma de San Luis Potosí, San Luis Potosí, Mexico; ²Facultad de Ciencias, Benemérita Universidad Autónoma de San Luis Potosí, San Luis Potosí, Mexico; ³Instituto de Investigación en Comunicación Óptica, Benemérita Universidad Autónoma de San Luis Potosí, San Luis Potosí, Mexico; ⁴Instituto de Física, Benemérita Universidad Autónoma de San Luis Potosí, San Luis Potosí, Mexico; ⁵Departamento de Conservación y Restauración de Bienes Culturales, Universitat Politècnica de València, Valencia, Spain

ABSTRACT

Focusing on the photographic archive of Julian Carrillo (Mexico), we study and characterize the photographic processes of a set of 13 photographs dated between 1884 and 1925. By using infrared spectroscopic ellipsometry, we classified a selected set of photographs according to its kind of binder. Thus, we recognized for each photograph, the presence of proteins, and therefore, the particular photographic process. Furthermore, we have identified the presence of baryta layer, the use of plasticizer, and the eventual coating utilized to protect the photograph, whose composition was based in natural organic components, mainly shellac, beeswax, or camphor.

ARTICLE HISTORY

Received September 2017
Accepted May 2018

KEYWORDS

Ellipsometry; photography; binders; historic archive; characterization; photographic processes

Introduction

Objectively identifying the stratigraphic structure and chemical composition of photographic prints, for which a great variety of processes have been developed since the invention of photography, poses in the present a full challenge that undermines some of the empirical assumptions employed by experts who work by visualization. An important part of the structure is the binder forming the matrix of the light-sensitive layer. The more common and more demanding identifications include albumen, collodion, and gelatin processes. Additionally, structural differences between them, and the possibility of containing dyes, varnishes, and other physical characteristics, can complicate their identification. For the preservation of late nineteenth-century and early twentieth-century photographs, it must be considered that these objects consist of multi-layer systems made up of complex mixtures of inorganic and organic materials. The fragility and vulnerability of both the photographs' supports and their thin overlayers prevent the analyst from performing a simple identification. The experimental techniques more commonly used in laboratory and conservation workshops are either destructive or insufficient.

A number of working methods have been developed and introduced to aid in the identification of photograph processes (Coe and Haworth-Booth 1983; Reilly 1986; Sammlung, Knodt, and Pollmeier 1999). Fourier transform infrared (FTIR) spectroscopy in

either transmission mode or attenuated total reflection (ATR), and micro FTIR have been used to detect organic compounds in photographs (Gernsheim 1965; Stulik et al. 2002; McCabe 2005; Ricci, Bloxham, and Kazarian 2007; Cattaneo et al. 2008; Casoli and Fornaciari 2014).

The employment of infrared absorbance spectroscopy provides information on the structural and compositional properties of the binder. Use of the binder was necessary at the time to protect silver particles from air pollution or other substances present in adjacent materials. Hence its use was an attempt to preserve the images from oxidation and any other kind of deteriorating processes (Gernsheim 1965; Casoli and Fornaciari 2014).

In this work, we present a nondestructive analysis of photographic positive prints that prevents loss of information about the natural organic layer used as a binder coating. Infrared spectroscopic ellipsometry (IRSE) is proposed as a reliable optical technique which due to its capability to resolve infrared-active vibrational bands is helpful for establishing criteria for the identification of organic compounds present in photographic prints. As far as we know, IRSE has not been used as a characterization technique for photographic processes.

IRSE in the spectral range from 300 to 4000 cm⁻¹ (33–2.5 μm, within the mid-infrared range of the electromagnetic spectrum) is used as the characterization tool in the present work. This optical technique can be broadly described as follows (Fujiwara 2007): a well-defined linear polarized light impinges a sample

Vibrational properties of small rhodium clusters: role of magnetism, charge state, and isomerization effects

Diana C. Navarro-Ibarra, Juan F. Aguilera-Granja, and Ricardo A. Guirado-López^a

Instituto de Física “Manuel Sandoval Vallarta”, Universidad Autónoma de San Luis Potosí, Álvaro Obregón 64, San Luis Potosí, S.L.P. 78000, Mexico

Received 12 December 2017 / Received in final form 27 April 2018

Published online 5 July 2018

© EDP Sciences / Società Italiana di Fisica / Springer-Verlag GmbH Germany, part of Springer Nature, 2018

Abstract. Extensive density functional theory calculations dedicated to analyze the structure, electronic properties, and vibrational behavior of small and positively charged rhodium clusters are presented. Following the experimental results of Harding et al. [D.J. Harding et al., *J. Chem. Phys.* **133**, 214304-1 (2010)] Rh_9^+ , Rh_{11}^+ , Rh_{12}^+ , and Rh_{13}^+ clusters are considered and the infrared (IR) spectra for various structural isomers is simulated. The calculations reveal a complex interplay between the distribution and intensity of the IR active frequencies with the atomic structure, magnetism, and charge state of the systems, as well as the crucial role played by high-energy isomers to explain experimental data. Based on a direct comparison between theory and experiment we predict that, for Rh_9^+ , a weighted average of simulated IR spectra corresponding to our lowest energy 9-atom cubic cluster and the closest in energy compact isomer can yield an acceptable agreement between theory and experiment. The possibility of considering mixtures of various IR spectra to explain the measured data is supported by nudged-elastic-band calculations that reveal the existence of inter-conversion processes between different isomers with relatively small energy barriers (~ 0.6 eV). In addition, the recent observation of bi-exponential decays in reactivity experiments of rhodium clusters interacting with N_2O species around those sizes also supports this claim. For Rh_{11}^+ and Rh_{12}^+ clusters, we also obtain that compact high-energy structures with low spin magnetizations are the ones having an IR spectra more in agreement with experiments. Finally for the most common compact and cubic Rh_{13}^+ clusters considered in the literature, for which there are no experimental IR spectra to compare with, well defined vibrational features are predicted which could help to identify the atomic configuration of this highly relevant structure.

1 Introduction

The analysis of the chemical and physical properties of small transition metal (TM) clusters has been the subject of intense research in the last decade [1]. Theoretical studies and experimental measurements on freestanding clusters have revealed a complex interplay between size and chemical composition with the magnetic order, reactivity, and electronic behavior in these systems. The cluster's atomic structure plays a fundamental role in the observed properties on a macroscopic scale, however, the determination of the atomic distribution and local bonding configurations in these sub nanometer-sized structures is very difficult to achieve. In recent years, the use of far-infrared spectroscopy in combination with density functional theory (DFT) calculations has been shown to provide a successful strategy to solve this problem [2–7]. The measured distribution and intensity of infrared (IR) active frequencies of small TM clusters embedded

in rare-gas matrices can be compared with the simulated spectra of model systems, providing reliable information concerning the structure of TM clusters synthesized in laser vaporization experiments. Successful applications of the previous methodology can be found in the works of Fielicke and collaborators where interesting structural trends on small (neutral and charged) vanadium [2,4], niobium [3,4,7], and rhodium [5,6] clusters are reported.

Vibrational spectroscopy experiments combined with the messenger atom tagging technique are delicate and high-precision measurements in which the adsorption of argon species on the surface of TM clusters can induce changes in the geometrical structure of the particles as well as variations in the location of the IR active frequencies and their corresponding intensities. Furthermore, the existence of structural isomerism is not obvious to infer and, in some cases, low levels of depletion are found resulting in noisy vibrational spectra that complicates the interpretation of the data. From the theoretical side, DFT calculations have revealed that the energy ordering of cluster isomers depends on the choice of the exchange-correlation

^a e-mail: guirado@ifisica.uaslp.mx

Original article:

**AN AUTOMATED METHOD FOR THE EVALUATION OF BREAST
CANCER USING INFRARED THERMOGRAPHY**

Antony Morales-Cervantes¹, Eleazar Samuel Kolosovas-Machuca^{2*}, Edgar Guevara^{2,5},
Mireya Maruris Reducindo³, Alix Berenice Bello Hernández³, Manuel Ramos García⁴,
Francisco Javier González²

¹ Facultad de Ciencias, Universidad Autónoma de San Luis Potosí, Av. Dr. Salvador Nava
Mtz. s/n, Zona Universitaria 78290, San Luis Potosí, SLP, México

² Coordinación para la Innovación y la Aplicación de la Ciencia y la Tecnología
Universidad, Autónoma de San Luis Potosí, Sierra Leona 550, Lomas 2da. Sección 78210,
San Luis Potosí, SLP, México

³ Unidad Académica de Ciencias Naturales, Universidad Autónoma de Guerrero, Carretera
Nal. Chilpancingo-Petaquillas, Ex Rancho Shalako 39105. Petaquillas, Guerrero, México

⁴ Hospital General "Dr Raymundo Abarca Alarcón" Chilpancingo, Carretera Federal
Chilpancingo- Zumpango. Paraje Tierras Prietas S/N, Guerrero, México

⁵ CONACYT-Universidad Autónoma de San Luis Potosí, Sierra Leona 550, Lomas 2da.
Sección 78210, San Luis Potosí, SLP, México

* Corresponding author: Eleazar Samuel Kolosovas-Machuca, Coordinación para la
Innovación y la Aplicación de la Ciencia y la Tecnología, Universidad, Autónoma de San
Luis Potosí, Sierra Leona 550, Lomas 2da. Sección 78210, San Luis Potosí, SLP, México.
E-mail: samuel.kolosovas@uaslp.mx

<http://dx.doi.org/10.17179/excli2018-1735>

This is an Open Access article distributed under the terms of the Creative Commons Attribution License
(<http://creativecommons.org/licenses/by/4.0/>).

ABSTRACT

Breast cancer is one of the major causes of death for women. Temperature measurement is advantageous because it is non-invasive, non-destructive, and cost-effective. Temperature measurement through infrared thermography is useful to detect changes in blood perfusion that can occur due to inflammation, angiogenesis, or other pathological causes. In this work, we analyzed 206 thermograms of patients with suspected breast cancer, using a classification method, in which thermal asymmetries were computed, the most vascularized areas of each breast were extracted and compared; then these two metrics were added to yield a thermal score, indicative of thermal anomalies. The classification method based on this thermal score allowed us to obtain the test sensitivity of 100 %, specificity of 68.68 %; a positive predictive value of 11.42 % and negative predictive value of 100 %. These results highlight the potential of thermography imaging as adjunctive tool to mammography in breast cancer screening.

Keywords: Breast cancer, infrared thermography, automated screening

INTRODUCTION

Breast cancer is one of the major causes of death for women (Rastghalam and

Pourghassem, 2016), affecting all social levels of the population. Breast cancer is the most common cancer type in Mexico and

Prototipo electromecánico didáctico para apoyar en la enseñanza sobre turbinas eólicas



Raúl Castillo Meraz¹, Roberto Carlos Martínez Montejano², Isaac Campos Cantón³, Carmen del Pilar Suarez Rodriguez¹

¹*Coordinación Académica Región Huasteca Sur, Universidad Autónoma de San Luis Potosí, Carretera Tamazunchale - San Martín Km. 5, C.P. 79960, Tamazunchale, San Luis Potosí, México.*

²*Unidad Académica Multidisciplinaria Zona Media, Universidad Autónoma de San Luis Potosí, Carretera Rioverde-San Ciro, Km 4, C.P. 79615, El Carmen, Rioverde, San Luis Potosí, México.*

³*Facultad de Ciencias, Universidad Autónoma de San Luis Potosí, C.P. 78000, Álvaro Obregón 64, Col. Centro, San Luis Potosí, San Luis Potosí, México.*

E-mail: raul.castillo@uaslp.mx

(Recibido el 13 de febrero de 2018, aceptado el 6 de noviembre de 2018)

Resumen

Este artículo describe el diseño y la implementación de un sistema experimental que estima la potencia eléctrica que se puede producir por el movimiento angular de un sistema mecánico el cual emula el comportamiento interno simplificado de una turbina eólica comercial; también muestra los principios fundamentales de la conversión de energía mecánica en eléctrica los cuales son las bases principales de la operación de dispositivos electromecánicos tales como los aerogeneradores. Se involucran algunos conceptos relacionados con asignaturas de Máquinas Eléctricas, Física, Energías Renovables, Electrónica de Potencia y Microcontroladores los cuales fueron aplicados por estudiantes de ingeniería que participaron en el desarrollo de este proyecto. El principal objetivo de este trabajo es desarrollar un sistema para aplicaciones didácticas que se pueda montar en condiciones interiores y pueda ser construido con elementos accesibles y componentes económicos.

Palabras clave: Energía Eólica, Máquina Eléctrica, Potencia Eléctrica, Potencia Mecánica, Enseñanza de la Física.

Abstract

This article describes the design and implementation of an experimental system that estimates the electric power that can be produced by the angular motion of a mechanical system that represents the physical behavior of a commercial wind turbine; also shows the fundamental principles of mechanical-into-electrical energy conversion which are the main basis of operation of electromechanical devices such as wind turbines. Some theoretical concepts related with subjects of electric machinery, physics, renewable energies, power electronics and micro controllers were verified by engineering students that participated in the development of this project. The main aim of this work is to develop a system for didactic applications that can be mounted at indoor conditions and can be constructed from a set of basic and cheap electrical components.

Keywords: Electric Machine, Electric Power, Mechanical Power, Physics Teaching, Wind Energy.

PACS: 07.05.Fb, 88.05.-b, 84.50.+d, 07.50.Ek: 01.30.Os, 01.40.-d, 45.20.D-

ISSN 1870-909

I. INTRODUCCIÓN

La principal motivación para el desarrollo de este experimento fue la demostración de la relación entre la velocidad de viento y la potencia eléctrica que es capaz de producir una turbina eólica pensado para estudiantes de ciencias e ingeniería a través de un prototipo experimental que emule el comportamiento mecánico y eléctrico básico de dichos sistemas los cuales son dispositivos capaces de convertir la energía eólica a energía eléctrica.

En años recientes, la tendencia de la producción de energía en el mundo ha cambiado drásticamente debido al colapso de los precios del petróleo dejando un mejor panorama para las energías renovables en el mercado. Casi la mitad de la energía eléctrica generada mundialmente en 2014 fue basada en fuentes renovables [1].

Adicionalmente, la demanda energética mundial está proyectada para crecer un 37% para el año 2040 [2]. Esto representa un verdadero reto para la comunidad mundial porque es necesario incrementar la generación de energía de todo el mundo y además también requiere que la

Evaluation of Psychoacoustic Annoyance and Perception of Noise Annoyance Inside University Facilities

Edgar Tristán-Hernández

Universidad Autónoma de San Luis Potosí, México. Facultad de Ciencias, Campus Pedregal. Av. Chapultepec 1570, Privadas del Pedregal.

Ignacio Pavón García and Juan Manuel López Navarro

Instrumentation and Applied Acoustics Research Group (I2A2), Polytechnic University of Madrid (UPM), Campus Sur, Carretera de Valencia, km. 7, 28031 Madrid.

Isaac Campos-Cantón

Universidad Autónoma de San Luis Potosí, México. Facultad de Ciencias, Campus Pedregal. Av. Chapultepec 1570, Privadas del Pedregal.

Eleazar Samuel Kolosovas-Machuca

Universidad Autónoma de San Luis Potosí, Coordinación para la Innovación y la Aplicación de la Ciencia y la Tecnología. Sierra Leona 550, Lomas 2^{da} Sección, 78210, San Luis Potosí, San Luis Potosí, México.

(Received 20 March 2015; accepted 10 February 2016)

The levels of noise produced in university facilities by students, increases the noise annoyance. The quality of life and the academic performance of university students could be influenced by this factor. Unfortunately, as far as methodology is concerned, there are no regulations or standards that allow for the correct evaluation of noise annoyance at educative facilities. In this work a method for the evaluation of noise annoyance and an indicator of noise annoyance are presented. In order to obtain a numerical value, a percentage index, and a verbal index that represents the noise annoyance in a specific area at university facilities, psychoacoustic annoyance (PA) and evaluation of perception of noise annoyance has been related. Resulting from this correlation an indicator of noise annoyance was proposed. The results were associated with this indicator. The method and the proposed indicator allow for deeper evaluation of noise annoyance and facilitate the development of appropriate actions against noise.

1. INTRODUCTION

The impact of noise on the quality of life of people is a topic of interest of many researchers. The works on this topic mainly focused on studying noise annoyance produced by urban sources and its influence on quality of life, and the physical and psychological health of the general population.¹⁻⁵ However, noise annoyance inside educational facilities at the university level is a topic that has not been deeply studied. Topics such as background noise levels in classrooms, speech intelligibility, isolation, and acoustic conditioning specially inside classrooms are the main study areas.⁶⁻⁹ There are several factors that influence the increase of noise in these places. Inside university facilities, the students themselves are the main source of noise. Throughout the day, students are involved in many activities inside the university facilities. At the university, usually, there are places with a large mass of students. This is why noise increases significantly and, consequently, the noise annoyance as well.¹⁰ This problem is worst mainly in places with inexistent acoustic treatment like common halls and hallways. Typically, noise annoyance is a parameter evaluated with objective and subjective methods, but currently, there are no regulations to evaluate this parameter. This is the reason why different methods to determine annoyance are used

in many studies.^{1,2,4,11-20} However, the method described by Fastl and Zwicker²¹ is used in many studies. This method is based on the calculation of psychoacoustic parameters such as loudness, roughness, sharpness, and fluctuation strength. These four parameters result in another parameter that evaluates the annoyance known as psychoacoustic annoyance (PA). On the other hand, another typical method is based on listening tests in combination with the application of questionnaires.²²⁻²⁵ Different kinds of questionnaires and different scales of evaluation were used in the existing studies.^{1,3,5,26} However, to standardize the evaluation of the response to noise, the International Commission of the Biological Effects of Noise (ICBEN) established a method based on a survey that was developed in different languages.²⁷ This survey is the result of the collaboration of different researchers from around the world and consists of two questions; each one of them has different scales (a 5-point verbal scale and an 11-points numerical scale), which will be explained later. Because of the importance of the effects of noise on health, quality of life, and school performance of university students, the noise sources and acoustic conditions in areas where students usually develop their daily activities should be studied. In addition, it is essential to develop the mechanisms that study and develop strategies and regulations applicable to students, an important population group.

Application of dynamical system theory in LC harmonic oscillator circuits: A complement tool to the Barkhausen criterion

International Journal of Electrical Engineering
Education
0(0) 1–15

© The Author(s) 2018

Reprints and permissions:

sagepub.co.uk/journalsPermissions.nav

DOI: 10.1177/0020720918770140

journals.sagepub.com/home/ije



Pablo Salas-Castro¹ ,
Fines Delgado-Aranda¹,
Edgar Tristán-Hernández¹,
Roberto C Martínez-Montejano²,
J S Murguía³ and
Isaac Campos-Cantón¹

Abstract

There are different types of electronic oscillators that have a wide variety of applications in areas such as computing, audio, communication, among others. One of these is the harmonic oscillators that generate an output sinusoidal signal. Due to the advantages of these, this paper proposes a methodology based on an analysis based on the dynamical system theory. This provides undergraduates a useful tool for a better understanding of the harmonic oscillators in order to design and implement accurately this kind of circuits. This tool complements the widely recognized Barkhausen criterion, which is a mathematical condition that must be satisfied by linear feedback oscillators. The analysis based on the dynamical system theory consists of obtaining a state matrix and its eigenvalues from the mathematical model of the oscillator circuits. The eigenvalues are adjusted to get an oscillator system, thus from this way, a set of

¹Instituto de Investigación en Comunicación Óptica, Facultad de Ciencias, UASLP, México

²Unidad Académica Multidisciplinaria Zona Media, UASLP, México

³Facultad de Ciencias, UASLP, México

Corresponding author:

Pablo Salas-Castro, Instituto de Investigación en Comunicación Óptica, Facultad de Ciencias, UASLP, San Luis Potosí, SLP, México.

Email: iepablosalas@hotmail.com

A didactic prototype to estimate the electric power produced by an angular motion

R. Castillo Meraz*, R.C. Martínez Montejano, I. Campos-Cantón and M.F. Martínez Montejano

Coordinación Académica Región Huasteca Sur (CARHS)

Universidad Autónoma de San Luis Potosí (UASLP).

Km. 5 Carretera Tamazunchale-San Martín, Zip Code 79960.

Tamazunchale, San Luis Potosí, México.

**e-mail: raul.castillo@uaslp.mx*

Received 21 November 2017; accepted 16 March 2018

This paper describes the design and implementation of an experimental system that estimates the electric power that can be produced by the angular motion showing the fundamental principles of mechanical-into-electrical energy conversion, which are the operation main basis of electromechanical devices such as wind turbines. Some theoretical concepts related with curricular subjects such as Electric machinery, Physics, Renewable Energies, Power Electronics and Microcontrollers, were verified by Science students that participated in this project achievement. The main aim of this work is to show a simplified system development for didactic applications that can be mounted at indoor conditions and can be constructed from a set of basic and cheap electrical components.

Keywords: Electric Power; Electric Motor; Mechanical Power; Synchronous Generator; Wind Energy.

Este trabajo describe el diseño y la implementación de un sistema experimental de tipo didáctico que puede estimar cuanta potencia eléctrica se produce por un movimiento angular, mostrando así, los principios fundamentales de la conversión de energía mecánica en eléctrica los cuales son básicos para el análisis de la operación de dispositivos electromecánicos como lo son los aerogeneradores. En este trabajo se muestran algunos principios básicos relacionados con las asignaturas de Máquinas Eléctricas, Física, Energías Renovables, Electrónica de Potencia y Microcontroladores. Durante el desarrollo de este trabajo, estos principios fueron verificados por estudiantes de licenciatura quienes participaron en el desarrollo y caracterización de este prototipo. El objetivo principal de este artículo es el de mostrar el desarrollo de un sistema simplificado para aplicaciones didácticas que puede ser implementado en condiciones controladas de laboratorio y puede construirse a partir de elementos sencillos y económicos.

Descriptores: Potencia Eléctrica; Motor Eléctrico; Potencia Mecánica; Generador Síncrono; Energía Eólica.

PACS: 07.05.Fb; 88.05.-b; 84.50.+d; 07.50.Ek

1. Introduction

During 2015, the world's energy tendency has changed drastically due to the collapse of oil prices leaving a better outlook for the renewable energy market. Almost half of the new global power generation capacity installed in 2014 was based on renewable sources [1].

Additionally, the world energy demand is projected to grow by 37% to the year 2040 [2]. This poses a real challenge to the world community because it is fundamental to increase the energy generation worldwide, but also requires that this energy does not impact even more the critical environmental conditions of the earth.

The renewable sources are an ideal option to deal with this problem. Nowadays, the wind energy is the most used renewable energy type (only below hydroelectric energy) and has been growing exponentially for the past decades. This fact is due to some advantages versus other renewable sources, like the high energy conversion high efficiency (compared to the photovoltaic cells) and his 24-hour generation.

In this context it is necessary to promote the study of this energy type at universities; it is also required to develop educational projects (with low cost) that help students under-

stand their operation and learning about renewable energies and its relation with other subjects like Electrical Machinery. Recently works had been focused on this topic [3,4].

The main motivation for this project development was the demonstration of the relation between the wind and the electric power, through an experimental and didactic prototype for engineering and science students, in order to introduce them to this renewable energy systems due to wind turbines recent popularity, which are devices capable to convert wind energy into electrical energy.

This paper focuses on a didactic system that is based on the wind turbines energy conversion principle and was designed for helping undergraduate students to understand this principle and power conversion.

The advantages of this system are that can be constructed from a simple and cheap set of electrical and mechanical components that does not requires special conditions like three phase sources, electrical isolation or similar stuff; its development and operation can be done at indoor conditions without interferences and its start up can be easily done by undergraduate students. On the other hand, its principal disadvantage consists that is a simplified system; power losses due to mechanical friction, leakage currents or other similar

Recibido: 07.02.2018 | Aceptado: 26.05.2018

Palabras clave: Célula excitable, dolor, modelo electrónica, modelo H-H y potencial de acción.

La investigación del dolor clínico en la UASLP

JUAN ALBERTO VÉRTIZ HERNÁNDEZ

vertizalberto@gmail.com

EGRESADO DE LA MAESTRÍA DE CIENCIAS APLICADAS, UASLP

ISAAC CAMPOS CANTÓN

FACULTAD DE CIENCIAS, UASLP

ÁNGEL ANTONIO VÉRTIZ HERNÁNDEZ

COORDINACIÓN ACADEMICA REGIÓN ALTIPLANO, UASLP

En el transcurso de los años se ha estudiado el dolor y se han identificado sus orígenes; éste ha sido tratado por diversas disciplinas, las corrientes filosóficas, la religión y la ciencia; una de estas perspectivas, la religiosa, considera que el dolor es un castigo de los dioses (Cabral, 1993); años más tarde, este concepto religioso y filosófico se consideró arcaico, ya que las investigaciones en la ciencia empezarían a tomar auge y formalidad al momento de explicar los diferentes procesos fisiológicos que resultaron en postulados acerca del dolor.



Rapid reflectance-anisotropy spectroscopy as an optical probe for real-time monitoring of thin film deposition

Cite as: AIP Conference Proceedings **1934**, 040001 (2018); <https://doi.org/10.1063/1.5024494>
Published Online: 08 February 2018

J. Ortega-Gallegos, L. E. Guevara-Macias, A. Lastras-Martínez, D. Ariza-Flores, R. E. Balderas-Navarro, and L. F. Lastras-Martínez



View Online



Export Online

ARTICLES YOU MAY BE INTERESTED IN

[Real-time optical monitoring of semiconductor epitaxial growth](#)

AIP Conference Proceedings **1934**, 040002 (2018); <https://doi.org/10.1063/1.5024495>

[Real-time reflectance-difference spectroscopy of GaAs molecular beam epitaxy homoepitaxial growth](#)

APL Materials **2**, 032107 (2014); <https://doi.org/10.1063/1.4868519>

[Optical detection of graphene nanoribbons synthesized on stepped SiC surfaces](#)

Journal of Applied Physics **122**, 035701 (2017); <https://doi.org/10.1063/1.4993453>

AIP | Conference Proceedings

Get **30% off** all print proceedings!

Enter Promotion Code **PDF30** at checkout



Real-time optical monitoring of semiconductor epitaxial growth

Cite as: AIP Conference Proceedings **1934**, 040002 (2018); <https://doi.org/10.1063/1.5024495>
Published Online: 08 February 2018

A. Lastras-Martínez, J. Ortega-Gallegos, L. E. Guevara-Macías, D. Ariza-Flores, O. Núñez-Olvera, R. E. López-Estopier, R. E. Balderas-Navarro, and L. F. Lastras-Martínez



View Online



Export Citations

ARTICLES YOU MAY BE INTERESTED IN

[Rapid reflectance-anisotropy spectroscopy as an optical probe for real-time monitoring of thin film deposition](#)

AIP Conference Proceedings **1934**, 040001 (2018); <https://doi.org/10.1063/1.5024494>

[Real-time reflectance-difference spectroscopy of GaAs molecular beam epitaxy homoepitaxial growth](#)

APL Materials **2**, 032107 (2014); <https://doi.org/10.1063/1.4868519>

[Note: A simple multi-channel optical system for modulation spectroscopies](#)

Review of Scientific Instruments **88**, 126107 (2017); <https://doi.org/10.1063/1.4998596>

AIP | Conference Proceedings

Get **30% off** all print proceedings!

Enter Promotion Code **PDF30** at checkout

The banner features a blue gradient background with a stylized open book at the bottom. The text is in white and yellow, with the discount code 'PDF30' highlighted in a yellow box.



Aging spectral markers of tequila observed by Raman spectroscopy

L. I. Espinosa-Vega, A. Belio-Manzano, C. A. Mercado-Ornelas, I. E. Cortes-Mestizo & Victor H. Mendez-Garcia

European Food Research and Technology
Zeitschrift für Lebensmittel-
Untersuchung und -Forschung A

ISSN 1438-2377

Eur Food Res Technol
DOI 10.1007/s00217-018-3203-4





Self-ordering of InAs nanostructures on (631)A/B GaAs substrates

Eric Eugenio-López^{1*}, Christian Alejandro Mercado-Ornelas¹, Pallavi Kisan Patil², Irving Eduardo Cortes-Mestizo¹, José Ángel Espinoza-Figueroa¹, Andrei Yu Gorbachev³, Satoshi Shimomura², Leticia Ithsmel Espinosa-Vega¹, and Víctor Hugo Méndez-García¹

¹Center for the Innovation and Application of Science and Technology, Universidad Autónoma de San Luis Potosí, C.P. 78210, San Luis Potosí, México

²Graduate School of Science and Engineering, Ehime University, Matsuyama 790-8577, Japan

³Optical Communications Research Institute, Universidad Autónoma de San Luis Potosí, C.P. 78210, San Luis Potosí, México

*E-mail: eugenio.lopez.eric@gmail.com

Received July 13, 2017; accepted October 26, 2017; published online January 17, 2018

The high order self-organization of quantum dots is demonstrated in the growth of InAs on a GaAs(631)-oriented crystallographic plane. The unidimensional ordering of the quantum dots (QDs) strongly depends on the As flux beam equivalent pressure (P_{As}) and the cation/anion terminated surface, i.e., A- or B-type GaAs(631). The self-organization of QDs occurs for both surface types along $[1\bar{1}3]$, while the QD shape and size distribution were found to be different for the self-assembly on the A- and B-type surfaces. In addition, the experiments showed that any misorientation from the (631) plane, which results from the buffer layer waviness, does not allow a high order of unidimensional arrangements of QDs. The optical properties were studied by photoluminescence spectroscopy, where good correspondence was obtained between the energy transitions and the size of the QDs. © 2018 The Japan Society of Applied Physics

1. Introduction

In the last decades, the growth of semiconductor self-assembled quantum dots (QDs) has been widely studied, since their delta-function-like density of states is very promising for future devices with advantageous characteristics such as enhanced performance and low power consumption.

However, the nucleation of InAs layers on GaAs substrates obtained via the Stranski–Krastanov (SK) growth mode with solid-source molecular beam epitaxy (MBE) results in the random arrangement of irregular sizes of quantum dots, thus impacting the device performance. Hence, to maximize the device performance, it is critical to control both the size homogeneity and the in-plane nucleation of the QDs.

Various research groups have worked on the optimization of appropriate conditions for controlling QD self-organization,^{1–3)} mostly on (100)-oriented substrates. Yet, owing to the stochastic nature of adatom nucleation, the spatial ordering of QDs is still extremely challenging. On the other hand, the MBE growth on high-index substrates (HIS) has been demonstrated to be an excellent alternative for obtaining corrugated surfaces,^{4,5)} which can be further used as templates to synthesize QDs.

Understanding the growth process on HIS can accomplish potential technological value improvements of practical devices and applications, such as low-threshold current density lasers,⁶⁾ 1.3- μm -wavelength laser diodes,⁷⁾ mode-locked lasers,⁸⁾ semiconductor saturable absorber mirrors (SESAMs),⁹⁾ and superluminescent light-emitting diodes,¹⁰⁾ among others.

In this work, the analysis of the self-assembly and self-organization of InAs QDs on GaAs(631)A- and B-type surfaces is reported. For the growth, the equivalent beam As pressure was varied and the effects on the QD morphology and their electron confinement were investigated.

2. Methods

Samples were grown in a vacuum generator (VG) Semicon MBE system using semi-insulating GaAs(631)A/B HIS. Prior to their loading into the VG chamber, the substrates were chemically etched in a “Semico Clean” solution

(Furuuchi Chemical) for 1 h. Once transferred to the growth chamber, the thermal desorption of GaAs fresh oxides was carried out at 640 °C for 20 min under As_4 flux. Then, a 0.5- μm -thick GaAs buffer layer (BL) was deposited at 700 °C at a growth rate (GR) of 0.3 $\mu\text{m}/\text{h}$. Afterwards, 3-ML InAs nanostructures were grown at a fixed temperature of 470 °C and a GR of 0.05 ML/s. The depositions were classified on the basis of three different As_4 beam equivalent pressures (P_{As}) used during their growth, namely, 3.0, 4.5, and 6.0×10^{-6} mbar. A second set of GaAs-capped samples were prepared for optical characterization purposes. Finally, the samples surface morphologies were investigated by atomic force microscopy (AFM) operated in contact mode, and the optical properties were studied by photoluminescence spectroscopy (PL) with a 532 nm photo-excitation source.

3. Results and discussion

The discussion starts by describing the A- and B-type GaAs surfaces, which differ from one another only by the topmost atoms, whether they are preferentially terminated in Ga or As, respectively. Figure 1(a) shows a ball-and-stick model of the bulk truncated two-dimensional GaAs(631) primitive cell.¹¹⁾ The primitive vectors $\mathbf{u}_1 \approx 2.2 a_{\text{GaAs}}[\bar{1}20]$ and $\mathbf{u}_2 \approx 1.6 a_{\text{GaAs}}[0\bar{1}3]$ are depicted in Fig. 1(a), where a_{GaAs} refers to the GaAs lattice constant. A similar primitive cell was previously presented;¹¹⁾ nonetheless, certain differences are proposed. To construct the cell crystal basis, all of the atoms that sustain free bonds after performing a cut of the zincblende structure were taken into consideration. The crystal basis contains both Ga and As atoms, but not all of them are located at the same height, which defines a periodically faceted surface as observed in Fig. 1(b). A simple electron-counting procedure shows that both types of surfaces have 12 free bonds per unit cell. The bonds are distributed in a 2 : 1 relation where the preferentially atom-terminated surface has the highest quantity of bonds. Therefore, the A face possesses 11 free electrons per unit cell, 6 atoms of Ga, and 3 atoms of As; similarly, the B face has 13 free electrons per unit cell, 3 atoms of As, and 6 atoms of Ga.

Figure 2 shows $2 \mu\text{m}^2$ AFM images of the InAs QDs grown at different P_{As} values over (631)A- and (631)B-



InAs quantum dots nucleation on (100) and anisotropic (631)-oriented GaAs substrates



E. Eugenio-López^a, M. Lopez-Lopez^b, A.Yu. Gorbachev^c, L.I. Espinosa-Vega^a, I.E. Cortes-Mestizo^a, C.A. Mercado-Ornelas^a, A. Del Río-De Santiago^d, Victor H. Méndez-García^{a,*}

^a Center for the Innovation and Application of Science and Technology, Universidad Autónoma de San Luis Potosí, Sierra Leona # 550, Lomas 2a Sección, San Luis Potosí 78210, Mexico

^b Physics Department, Centro de Investigación y de Estudios Avanzados del Instituto Politécnico Nacional, Av. Instituto Politécnico Nacional # 2508, San Pedro Zacatenco, Distrito Federal 07360, Mexico

^c Optical Communications Research Institute, Universidad Autónoma de San Luis Potosí, Av. Karakorum # 1470, Lomas 4ª Sección, San Luis Potosí 78210, Mexico

^d Academic Unit of Engineering, Universidad Autónoma de Zacatecas, Ramón López Velarde # 801, Zacatecas Centro, Zacatecas 98000, Mexico

ARTICLE INFO

Keywords:

Molecular beam epitaxy
InAs quantum dots
Self-alignment
Anisotropic high index substrates
Nucleation
Corrugated surfaces

ABSTRACT

Different mechanisms of adatoms nucleation are studied for the self-assembling of InAs quantum dots (QDs) on smooth and nanoscale faceted GaAs surface morphologies. The experiments were performed on GaAs(100) and GaAs(631), and prior to the arrival of InAs the GaAs surface morphology was intentionally altered by changing the growth temperature of the buffer layer, T_{BL} . For the reflection high-energy electron diffraction (RHEED) analysis, an equilibrium interlayer mass transport model is proposed through which, the critical thickness (H_c) and the InAs diffusion length can be estimated. For InAs growth on (100) substrates the H_c did not show significant dependence on T_{BL} , but the adatoms diffusion length slightly reduced as T_{BL} increases, which is in agreement with the changes on QDs density as observed by atomic force microscopy (AFM). For samples grown on GaAs (631)-oriented substrates it was found that both the nucleation mode of InAs and the H_c depends on T_{BL} . The changes are associated to the growth of InAs on GaAs surface faceted corrugation that allows the self-organizing InAs QDs along [-113].

1. Introduction

In(Ga)As semiconductor quantum dots (QDs) are actively studied due to their potential applications in a variety of devices, such as 1.3 μm wavelength laser diodes [1,2], modelocked lasers [2], semiconductor saturable absorber mirrors (SESAMs) [3], super luminescent light emitting diodes [4], among others [5]. The most current approach for the synthesis of these nanostructures is based on the self-assembled QDs obtained by Stransky-Krastanow (SK) growth. This method governed by stress, which has been mostly studied on GaAs (100)-oriented substrates [6–10], offers limited control on shape, size and composition of the QDs, and no control on their nucleation sites on the substrate surface. Therefore, in order to improve the QDs-based devices mechanisms for the surface arrangement of these zero-dimensional structures must be studied, which leads to the searching for self-organization processes. The use of high index substrates is a good alternative for QDs self-organization because surface corrugation can be promoted by their natural high surface anisotropy and instability

under suitable growth conditions. If the dimensions of the terraces that conforms such corrugation is driven towards the nanoscale regimen, they can serve as one-dimensional (1D) templates for the post growth of InAs, and consequently to their 1D arrangement [11,12]. It is worth to comment that both the QDs synthesis via the SK growth mode and the nanoscale corrugation formation are self-assembly processes mainly promoted by strain [13,14]. Therefore when these stress singularities are combined the kinetics and thermodynamics of the nucleation and growth turn out to be as complex as interesting.

In this work the nucleation mechanisms of InAs quantum dots on isotropic (100) and anisotropic (631) GaAs substrates are studied. Reflection high-energy diffraction (RHEED) was utilized to study the strain relaxation mechanisms occurring during the InAs growth by proposing a model of interlayer mass transport, which was successfully applied to the InAs/GaAs(100) 2D-3D growth mode transition. In addition, the InAs nucleation is studied on GaAs surface faceted buffer layers. In spite of the interface strain originated by the InAs/GaAs lattice mismatch, unidimensional alignment of self-assembled InAs

* Corresponding author.

E-mail address: vyktormen@gmail.com (V.H. Méndez-García).

Brief Analysis of the Optical Behavior of ZnS: Mn Nanocrystals

^{1, 9} Ortiz Hernández A.A., ^{*2} Durán Muñoz H.A., ³ Hernández Ortiz M., ² Berumen Torres J.A., ⁴ Méndez García V.H., ⁵ Ortega Sígala J.J., ⁵ Pérez Arrieta M. L., ⁶ Guzmán García K.A., ⁷ Alfaro Cruz M.R., ⁸ Vega Carrillo H.R.

¹ Carrera de Ingeniería en Mecatrónica. Universidad Politécnica de Zacatecas, UPZ, ² Carrera de Ingeniería Industrial. Universidad Politécnica de Zacatecas, UPZ, ³ Unidad Académica de Economía, Universidad Autónoma de Zacatecas, ⁴ Coordinación para la Innovación y Aplicación de la Ciencia y la Tecnología, UASLP, ⁵ Unidad Académica de Física, Universidad Autónoma de Zacatecas, ⁶ Universidad Politécnica de Madrid, Departamento de Ingeniería Nuclear, Madrid España, ⁷ Centro de Investigación en Materiales Avanzados, Apodaca, México and ⁸ Unidad Académica de Estudios Nucleares, Universidad Autónoma de Zacatecas, ⁹AORTech, Research Department, C. Purisima #227, Lomas de Cristo, Zacatecas, Zac., Mex. 98085.


Abstract

Depending on the particle size of the zinc sulfide (ZnS), some optical properties may change. In particular, the inclusion of manganese (Mn²⁺) as an impurity shows interesting optical properties, which has become a topic of interest. Therefore, it is necessary to perform a complementary optical characterization of the ZnS: Mn nanocrystals. In this work was analyzed by different techniques of characterization the optical behavior of ZnS: Mn nanocrystals. We found that the sample doped with a concentration of 10% shows the highest luminescent response. It was also observed an atomic rearrangement using thermal treatments above 500 °C, resulting in a cubic-to-hexagonal (Wurtzite) phase transition. Finally, the shape and position of the experimental TL glow curves are analyzed using the glow curve deconvolution technique, in order to characterize the transfer of electrons observed in the nanocrystals.

Keywords: ZnS:Mn nanocrystals, thermoluminescence and glow curve deconvolution.

* Corresponding author: hectorduranm@hotmail.com

Design of a strong S-box based on a matrix approach

J. A. Aboytes-González · J. S. Murguía  ·
M. Mejía-Carlos · H. González-Aguilar ·
M. T. Ramírez-Torres

Received: 19 October 2017 / Accepted: 8 July 2018 / Published online: 18 July 2018
© Springer Nature B.V. 2018

Abstract In this paper, we present a matrix approach based on the rule 90 cellular automata, and a fractional linear transformation over Galois field $GF(2^8)$, to implement a strong substitution box (S-box). To make the assessment of this proposal, some standard tests are performed, and the obtained numerical results show that this proposed S-box is comparable or superior to some S-boxes used as benchmarks in this work. Also, to measure the strength of the S-box in image encryption, some statistical tests are carried out, which prove that our proposal exhibits appealing security properties.

Keywords S-box · Cellular automaton · Cryptography

1 Introduction

Nowadays, we count with several classes of encryption systems to protect different kinds of information, which are based on various approaches such as Data Encryption Standard (DES), Advanced Encryption Standard (AES), International Data Encryption Algorithm (IDEA), among others [1–3].

Some of these popular encryption systems are classified as block ciphers, in which plaintext–ciphertext blocks are of a fixed length, and the key size may be different; for instance, the plaintext–ciphertext blocks of the AES are 128 bits in length and the key size may be 128, 192, or 256 bits. One of the main characteristics of block ciphers is to achieve the property referred as confusion, a term defined by Shannon in 1949 [4]. Such a property makes the statistical relationship between the ciphertext and the key as difficult as possible, and this is attained by means of a substitution table commonly known as a substitution box (S-box). In general, the S-box is the nonlinear component in such systems; therefore, they are essential in the encryption process. Moreover, the employment of S-boxes in many applications has shown a good performance. For instance, References [5,6] consider S-boxes in image encryption applications obtaining positive results; in [7], the authors use the S-box for watermarking applications, whereas in [8] are used for

J. A. Aboytes-González · M. Mejía-Carlos
Instituto de Investigación en Comunicación Óptica,
Universidad Autónoma de San Luis Potosí (UASLP),
Álvaro Obregón 64, 78000 San Luis Potosí, S.L.P., Mexico
e-mail: j.a.a.g.85@hotmail.com

M. Mejía-Carlos
e-mail: marcela.mejia@uaslp.mx

J. S. Murguía (✉) · H. González-Aguilar
Laboratorio Nacional CI3M, Facultad de Ciencias,
Universidad Autónoma de San Luis Potosí (UASLP),
Álvaro Obregón 64, 78000 San Luis Potosí, S.L.P., Mexico
e-mail: ondeleto@uaslp.mx

H. González-Aguilar
e-mail: hernan@fc.uaslp.mx

M. T. Ramírez-Torres
Coordinación Académica Región Altiplano Oeste,
Universidad Autónoma de San Luis Potosí (UASLP),
Carretera Salinas-Santo Domingo # 200 Salinas, San Luis
Potosí, Mexico
e-mail: tulio.torres@uaslp.mx



Oxidative dehydrogenation of n-octane over Mg-containing SBA-15 material

Eliena Gaxiola^a, F. F. Castellón^b, José A. Hernández^c, B. Acosta^b, J. N. Díaz de León^b, S. Fuentes^b and T. A. Zepeda^b

^aPosgrado en Ciencia e Ingeniería de los Materiales, Centro de Nanociencias y Nanotecnología, Universidad Nacional Autónoma de México, Ensenada, México; ^bUniversidad Nacional Autónoma de México, Centro de Nanociencias y Nanotecnología, Ensenada, México; ^cUPIIC, del Instituto Politécnico Nacional, Silao de la Victoria, México

ABSTRACT

In this study, it is proposed the incorporation of MgO into of SBA-15 via the direct synthesis different atomic ratios of Si/Mg (20, 40 and 80). Although the incorporation of Mg did not affect the mesoporous character of SBA-based materials, it was found dramatic changes in the SBA-15 characteristic honeycomb structure even after the incorporation of small amount of Mg. The creation of more basic sites in SBA-15, because of the addition of Mg, improved ODH conversion of n-octane with respect to SBA-15, used as reference. Sample with a Si/Mg molar ratio of 20 showed the best catalytic performance in the oxidative dehydrogenation of n-octane, while the sample with a Si/Mg molar ratio of 40 achieve the highest productions of olefins.

ARTICLE HISTORY

Received 28 June 2016
Accepted 1 March 2017

KEYWORDS

Mesoporous silica SBA-15;
Mg-SBA-15; oxidative
dehydrogenation of
n-octane

1. Introduction

The oxidative dehydrogenation (ODH) of alkanes have become in one of the most interesting reactions in the petrochemical industry to mainly produce olefins and aromatics, the most important raw materials in a wide range of applications due to their low cost and ability to be easily functionalised. The ODH reaction is known due to its high activity and selectivity, low carbon deposition and a low cost in comparison to the reaction without oxygen [1–5].

ODH catalytic performance relies on the acid-base properties of the catalyst material and isolated cations capable of activating C–H bonds [6–9], therefore the use of supports with acid-base characteristics is advantageous. C⁴-olefins are considered basic and nucleophilic for its high electron densities in π bonds. Then basic oxides do not absorb strongly olefins and the selectivity is relatively high, while acidic oxides, adsorb strongly olefins and promotes oxidation to carbon oxides [10]. Since 1990s have been published many reviews and papers devoted to the ODH of light alkanes using vanadium, molybdenum, tungsten and niobium oxides as active phase [11–13], where silica-based materials (with different structures) are among the most used supports [10].

Mesoporous silica SBA-15 has attracted much attention as support due their ordered hexagonal structure with high surface area of 600–1000 m²/g, pore sizes adjustable of 4.6 to 30 nm and wall thickness of 3.1 to 6.4 nm [14,15]. In some works, SBA-15 was modified with different atoms, like Cr–Ce, in the ODH of ethane to ethylene [16], vanadium in the ODH of propane to propylene [17], and with aluminium and titanium, in reactions of hydrodesulphurisation of dibenzothiophene (HDS of DBT) and hydrogenation of biphenyl [18,19]. Some researchers also have been introduced other atoms into the structure of SBA-15. Li et al. using the direct synthesis method with controlled hydrolysis (performed only with pH adjustment), reached incorporation of Al and Ti ions which

resulted in a significant changes in the catalytic properties [20]. SBA-15 was also doped with lanthanum, by direct synthesis and post-synthesis. The incorporation of significant amount of lanthanum was achieved by post-synthesis procedure obtaining that mesoporous molecular sieves retain the hexagonal order and physical properties of siliceous SBA-15 material [21].

In the other hand, magnesium oxide is considered a basic compound and mesoporous silica SBA-15 is a neutral material, then using MgO on mesoporous silica SBA-15 will maintain the basic character, and can be a suitable catalyst for the reaction of alkanes ODH. To the best of our knowledge, although MgO is reported as support for the ODH of light alkanes, the incorporation of Mg ions into the SBA-15 structure has not been proposed yet in the ODH of n-octane. In this paper, mesoporous silica SBA-15 was doped with magnesium by direct synthesis in order to avoid the leaching of the structure. Incorporation of magnesium preserves the basic character, with great potential to catalyse oxidative dehydrogenation alkanes of long chain such as n-octane.

2. Experimental methods

2.1. Synthesis of SBA-15 and Mg-SBA-15 materials

The pure SBA-15 was synthesised using tetraethyl orthosilicate (TEOS, Sigma Aldrich) as silica source and nonionic triblock copolymer surfactant EO₂₀PO₇₀EO₂₀ (P123, Aldrich) as a structure-directing agent, as in [22]. Typically, 4 g of P123 was dissolved in 150 mL of aqueous HCl at pH 1.5. Subsequently, 5 mL of TEOS was added dropwise to the solution. After stirring at 40 °C for 24 h, the mixture was aged at 80 °C for 24 h. The white precipitate was then collected by filtration and dried at 110 °C overnight. The product was obtained by removing the template at 550 °C for 6 h at a heating rate of 1 °C/min.

Mg-SBA-15 materials were synthesised using tetraethyl orthosilicate (TEOS, Sigma Aldrich) and magnesium ethoxide



Preparation of air stable nanoscale zero valent iron functionalized by ethylene glycol without inert condition



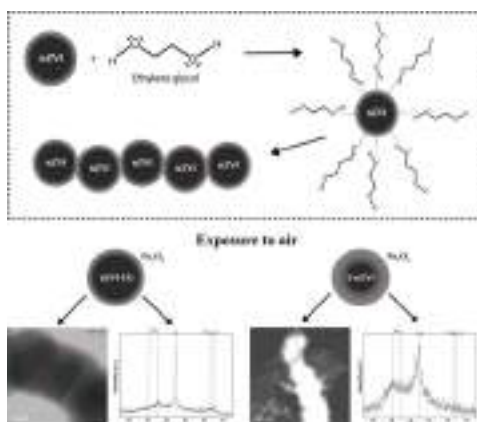
Claudio Adrian Ruiz-Torres^a, René Fernando Araujo-Martínez^a, Gabriel Alejandro Martínez-Castañón^a, J. Elpidio Morales-Sánchez^a, Jesús María Guajardo-Pacheco^a, Jesús González-Hernández^b, Tae-Jin Lee^c, Hyun-Sang Shin^c, Yuhon Hwang^{c,*}, Facundo Ruiz^{a,*}

^a Facultad de Ciencias, Universidad Autónoma de San Luis Potosí (UASLP), Avenida Manuel Nava 6, Zona Universitaria, C.P. 78290 San Luis Potosí, SLP, Mexico

^b Centro de Ingeniería y Desarrollo Industrial (CIDESI), Av. Playa Pie de la Cuesta No. 702, Desarrollo San Pablo, C.P. 76125 Santiago de Querétaro, Qro, Mexico

^c Department of Environmental Engineering, Seoul National University of Science and Technology, 232 Gongreung-ro, Nowon-gu, Seoul 01811, Republic of Korea

GRAPHICAL ABSTRACT



ARTICLE INFO

Keywords:

Ethylene glycol
Nanoscale zero-valent iron (nZVI)
Functionalization
Colloidal stability

ABSTRACT

The use of nanoscale zero-valent iron has been widely studied in recent years for potential application in environmental engineering, due to its affinity for a large number of contaminants, which may be in aqueous or solid phase, and for its abundance, which makes it an attractive tool for environmental remediation. However, there exist some variables in the production of nZVI that complicate the generation of the material, such as the complex methodologies of synthesis and the cost of inert conditions like nitrogen or argon atmosphere, which have the purpose of preventing the oxidation and reducing the instability of the material under ambient conditions. As a simple and economical synthesis methodology, this work presents an optimized method to synthesize functionalized nanoscale zero-valent iron (nZVI) using ethylene glycol (EG) without need for inert conditions. The coordination of iron ions during the nZVI-EG synthesis and the functionalization mechanism of the nanoparticles were identified by UV–Vis absorption spectroscopy and Fourier transform infrared spectroscopy (FTIR). Functionalized nZVI showed increased dispersibility due to the effects of steric repulsion between the grafted polymers. Ethylene glycol functionalized nZVI showed stability against oxidation during dry atmospheric condition, while significant oxidation was observed in the case of unfunctionalized nZVI. This result

* Corresponding authors.

E-mail addresses: yhwang@seoultech.ac.kr (Y. Hwang), facundo@ciencias.uaslp.mx (F. Ruiz).

<https://doi.org/10.1016/j.cej.2017.11.047>

Received 28 August 2017; Received in revised form 31 October 2017; Accepted 8 November 2017

Available online 11 November 2017

1385-8947/ © 2017 Elsevier B.V. All rights reserved.



Contents lists available at ScienceDirect

Data in Brief

journal homepage: www.elsevier.com/locate/dib



Data Article

Effect of the reaction medium on the characteristics of silanized titanium dioxide particles: Differences obtained in the Zeta potential data and infrared spectra



E. Delgado Alvarado ^a, L. López-Zamora ^b, Cristina Pérez Pérez ^c,
E. Pérez ^d, J.A. Vazquez-Lopez ^e, J.A. González-Calderón ^{e,*}

^a Doctorado Institucional en Ingeniería y Ciencias de Materiales, Universidad Autónoma de San Luis Potosí, Zona Universitaria, Av. Dr Manuel Nava s/n, Lomas, C.P. 78290 San Luis Potosí, SLP, Mexico

^b División de Estudios de Posgrado e Investigación. Tecnológico Nacional de México/Instituto Tecnológico de Orizaba, Av. Oriente 9 No. 852. Col. Emiliano Zapata, C.P. 94320 Orizaba, Veracruz, Mexico

^c Departamento de Ingeniería Bioquímica, Instituto Tecnológico de Celaya, Av. Tecnológico y Antonio García Cubas s/n, C.P. 38010 Celaya, Gto, Mexico

^d Instituto de Física, Universidad Autónoma de San Luis Potosí, Zona Universitaria, Av. Dr. Manuel Nava s/n, Lomas, C.P. 78290 San Luis Potosí, SLP, Mexico

^e Departamento de Ingeniería Industrial, Instituto Tecnológico de Celaya, Av. Tecnológico y Antonio García Cubas s/n, C.P. 38010 Celaya, Gto, Mexico

ARTICLE INFO

Article history:

Received 18 September 2018

Received in revised form

17 October 2018

Accepted 22 October 2018

Available online 26 October 2018

ABSTRACT


In this document we present the differences in the Zeta potential and in the Infrared spectra data obtained from the characterization of silanized titanium dioxide particles, using two different solvents as reaction media: ethanol and toluene. Also, we provide micrographs of transmission electron microscopy in order to show morphological differences between the analyzed samples.

© 2018 The Authors. Published by Elsevier Inc. This is an open access article under the CC BY license (<http://creativecommons.org/licenses/by/4.0/>).

* Corresponding author.

E-mail address: amir.gonzalez@iqcelaya.itc.mx (J.A. González-Calderón).

Design of a strong S-box based on a matrix approach

J. A. Aboytes-González · J. S. Murguía  ·
M. Mejía-Carlos · H. González-Aguilar ·
M. T. Ramírez-Torres

Received: 19 October 2017 / Accepted: 8 July 2018 / Published online: 18 July 2018
© Springer Nature B.V. 2018

Abstract In this paper, we present a matrix approach based on the rule 90 cellular automata, and a fractional linear transformation over Galois field $GF(2^8)$, to implement a strong substitution box (S-box). To make the assessment of this proposal, some standard tests are performed, and the obtained numerical results show that this proposed S-box is comparable or superior to some S-boxes used as benchmarks in this work. Also, to measure the strength of the S-box in image encryption, some statistical tests are carried out, which prove that our proposal exhibits appealing security properties.

Keywords S-box · Cellular automaton · Cryptography

1 Introduction

Nowadays, we count with several classes of encryption systems to protect different kinds of information, which are based on various approaches such as Data Encryption Standard (DES), Advanced Encryption Standard (AES), International Data Encryption Algorithm (IDEA), among others [1–3].

Some of these popular encryption systems are classified as block ciphers, in which plaintext–ciphertext blocks are of a fixed length, and the key size may be different; for instance, the plaintext–ciphertext blocks of the AES are 128 bits in length and the key size may be 128, 192, or 256 bits. One of the main characteristics of block ciphers is to achieve the property referred as confusion, a term defined by Shannon in 1949 [4]. Such a property makes the statistical relationship between the ciphertext and the key as difficult as possible, and this is attained by means of a substitution table commonly known as a substitution box (S-box). In general, the S-box is the nonlinear component in such systems; therefore, they are essential in the encryption process. Moreover, the employment of S-boxes in many applications has shown a good performance. For instance, References [5,6] consider S-boxes in image encryption applications obtaining positive results; in [7], the authors use the S-box for watermarking applications, whereas in [8] are used for

J. A. Aboytes-González · M. Mejía-Carlos
Instituto de Investigación en Comunicación Óptica,
Universidad Autónoma de San Luis Potosí (UASLP),
Álvaro Obregón 64, 78000 San Luis Potosí, S.L.P., Mexico
e-mail: j.a.a.g.85@hotmail.com

M. Mejía-Carlos
e-mail: marcela.mejia@uaslp.mx

J. S. Murguía (✉) · H. González-Aguilar
Laboratorio Nacional CI3M, Facultad de Ciencias,
Universidad Autónoma de San Luis Potosí (UASLP),
Álvaro Obregón 64, 78000 San Luis Potosí, S.L.P., Mexico
e-mail: ondeleto@uaslp.mx

H. González-Aguilar
e-mail: hernan@fc.uaslp.mx

M. T. Ramírez-Torres
Coordinación Académica Región Altiplano Oeste,
Universidad Autónoma de San Luis Potosí (UASLP),
Carretera Salinas-Santo Domingo # 200 Salinas, San Luis
Potosí, Mexico
e-mail: tulio.torres@uaslp.mx

Wavelet characterization of hyper-chaotic time series

J.S. Murguía^a, H.C. Rosu^b, L.E. Reyes-López^c, M. Mejía-Carlos^c, and C. Vargas-Olmos^c

^a Facultad de Ciencias, Universidad Autónoma de San Luis Potosí (UASLP),
Alvaro Obregón 64, 78000 San Luis Potosí, S.L.P., México.

^b IPICYT, Instituto Potosino de Investigación Científica y Tecnológica,
Camino a la presa San José 2055, Col. Lomas 4a Sección, 78216 San Luis Potosí, S.L.P., México.

^c Instituto de Investigación en Comunicación Óptica, UASLP,
Alvaro Obregón 64, 78000 San Luis Potosí, S.L.P., México.

Received 5 November 2017; accepted 19 January 2018

A wavelet scaling numerical characterization of time series based on the variance of the wavelet coefficients is used for three well-known four-dimensional and one five-dimensional hyper-chaotic systems. We report several scaling behaviors for the variables of these hyper-chaotic systems.

Keywords: Hyper-chaotic time series; discrete wavelet transform; wavelet variance; scaling analysis.

En este trabajo se realiza una caracterización de escala numérica de series de tiempo hiper-caóticas basada en la varianza de los coeficientes ondeleta de tres sistemas hiper-caóticos conocidos de cuatro-dimensiones y uno de cinco-dimensiones. Se reportan los diferentes comportamientos de escala de las variables de estos sistemas hiper-caóticos.

Descriptor: Series de tiempo hiper-caóticas; transformada ondeleta discreta; varianza ondeleta; análisis de escala.

PACS: 05.45.-a; 05.45.Tp

1. Introduction

The wavelet transform (WT) is a mathematical tool for analyzing (decomposing) or synthesizing (reconstructing) a wide variety of generic signals at different frequencies and with different resolutions. In the wavelet analysis, a signal is decomposed into a type of functions called wavelets, which are translated and scaled versions of a finite-length and fast-decaying oscillating waveform. The latter is usually referred to as the analyzing wavelet basis function, or simply the mother wavelet. Similar to its preceding Fourier analysis, the wavelet analysis also contains various, closely-related forms of its transform, namely the continuous wavelet transform, the wavelet series, and the orthonormal discrete wavelet transform or, for short, the discrete wavelet transform (DWT). However, the most common choice to perform the analysis and synthesis of the original signal is the DWT because of the enormous versatility for computational calculations offered through its multiresolution filter bank structure [1, 2]. Just as in the other existent formats of the wavelet transform, the DWT is endowed with temporal resolution as a unique key advantage over its Fourier transform counterpart which allows to capture both the frequency and location information of the raw signal being processed in this way.

To the best of our knowledge, the class of hyper-chaotic systems, *i.e.*, those dynamical systems having at least two positive Lyapunov exponents, have not been directly studied by means of wavelet transforms. This motivated us to provide here a wavelet scaling analysis of four hyper-chaotic systems, of which three are four-dimensional – Chen, Chua, and Rössler – and one is a recently introduced five-dimensional system. All these systems are reviewed in Sec. 2, where we briefly present their systems of equations and attractors for

values of the parameters corresponding to the hyper-chaotic regime. Section 3 is devoted to a short description of the DWT. The main results are in Sec. 4, where we apply the wavelet analysis to the time series (TS) of the variables of these systems when they are in the hyper-chaotic regime. The paper ends up with a short conclusion section.

2. Hyper-chaotic systems

This section is devoted to a brief presentation of the four hyper-chaotic systems which we will consider in this work. These systems, despite their relative simplicity, exhibit a more complex dynamics than the chaotic systems, and they have received wide coverage in different areas of mathematics, physics, and engineering, among others [3–9].

2.1. Hyper-chaotic Chen system

The hyperchaotic dynamics of Chen's system is modeled by the set of differential equations [4, 6]

$$\begin{aligned}\dot{x} &= a(y - x), \\ \dot{y} &= x(d - z) + cy - w, \\ \dot{z} &= xy - bz, \\ \dot{w} &= x + k,\end{aligned}\tag{1}$$

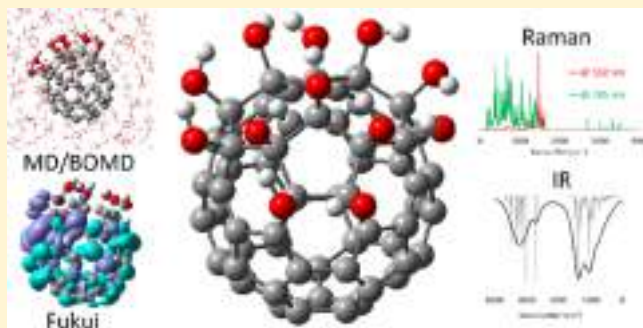
where a , b , c , d and k are parameters of the system. If $a = 36$, $b = 3$, $c = 28$, $d = -16$ and $-0.7 \leq k \leq 0.7$, the system (1) is in the hyper-chaotic regime. In fact, to check the existence of hyper-chaos, there must be at least two positive Lyapunov exponents. The numerically calculated exponents

Low Hydroxylated Fullerenes: Stability, Thermal Behavior, and Vibrational Properties

M. V. Velarde-Salcedo,[†] M. Gallo,[‡] and R. A. Guirado-López^{*,†}[†]Instituto de Física “Manuel Sandoval Vallarta”, Universidad Autónoma de San Luis Potosí, Álvaro Obregón 64, San Luis Potosí, S.L.P. 78000, Mexico[‡]Tecnológico Nacional de México/ITCJ, Av. Tecnológico 1340, Cd. Juárez, Chihuahua 32500, Mexico

Supporting Information

ABSTRACT: Extensive density functional theory (DFT) calculations dedicated to analyze the stability, thermal behavior, as well as the infrared (IR) and Raman spectra of low hydroxylated $C_{60}(OH)_{12}$ fullereneols are presented. Adsorbed configurations in which OH groups form various types of molecular islands on the carbon surface are the preferred atomic arrays, while random distributions of hydroxyl species are the highest energy molecular structures. It is found that the formation of local networks of hydrogen-bonded OH groups plays a fundamental role in the stability of these complexes. The calculated dipole moments, polarizability values, optical gap, and Fukui functions of $C_{60}(OH)_{12}$ isomers strongly depend on the structure of the hydroxyl overlayer, thus being an important parameter to tune the material properties. DFT Born–Oppenheimer molecular dynamics calculations at $T = 300$ K reveal that aggregated forms of OH groups on the fullerene surface show an interesting dynamical behavior, characterized by a continuous proton-exchange process between neighboring hydroxyl molecules that modifies the structure and chemical nature of the molecular coating. From nudged elastic band studies analyzing OH diffusion on the C_{60} surface, energy barriers opposing OH migration of ~ 1 eV are found. However, in the presence of surrounding H_2O species, a water-assisted diffusion process is obtained which can reduce the energy barriers to values as low as 0.25 eV. The comparison between experimental and calculated IR spectra of various $C_{60}(OH)_{12}$ isomers shows well-defined spectral features which can be very helpful to identify the structure of these fullerene complexes. Finally, simulations of the wavelength-dependent Raman spectra of hydroxylated fullerenes reveals (i) that the intensities of the Raman active modes strongly depend on the excitation laser and (ii) the importance of the wavelength-dependent calculations to reveal precise features of different regions of the spectra. The combination of IR and Raman spectroscopies is an efficient approach to reveal the atomic structure of these sub-nanometer-sized carbon nanostructures.



1. INTRODUCTION

In the last years, it has been clearly established that the functionalization of both inner and outer surfaces of carbon nanostructures dramatically changes their chemical, electronic, and transport properties.^{1–3} In particular, the attachment of hydrophilic substituents, such as OH groups, are of fundamental importance and provide an interesting route for the development of novel materials. For example, $C_{60}(OH)_{24}$ fullereneol structures can work as antioxidative agents⁴ and free radical scavengers,⁵ and recently, the potential application of fullereneols in cancer drug delivery has been reported.⁶ The functionalization of carbon nanotubes with polar groups can be used to improve dispersion as well as the chemical interaction with a polymer matrix.⁷ OH adsorption on single-walled carbon nanotubes modifies their electronic properties, which makes them good candidates for the design of novel electronic devices.⁸ Finally, hydroxyl-functionalized graphene has been recently synthesized.⁹ It shows good hydrophilicity and biocompatibility to human retinal pigment epithelium cells.¹⁰

It also provides an effective microenvironment for cell adhesion and proliferation.¹¹ In addition, hydroxylated graphene sheets can self-assemble to form flexible films with high electrical conductivity which can be used for high-power electronic applications.¹² It is important to emphasize that, after hydroxyl adsorption, it is possible to link more complex reagents such as aminoacids, DNA, and various types of drugs, leading also to strong changes in the solubility of the different nanocarbons.

In particular, hydroxylated fullerenes or fullereneols can be synthesized by various (and relatively simply) methods reported in the literature involving thermal treatments in the presence of HNO_3/H_2SO_4 mixtures,¹³ different hydrolysis procedures,¹⁴ as well as synthetic approaches using alkaline media and halogens as intermediates.^{15,16} However, all these techniques generally lead to the formation of OH-covered C_{60}

Received: February 15, 2018

Revised: May 9, 2018

Published: May 30, 2018

ARTICLE

Levi's Lemma, pseudolinear drawings of K_n , and empty triangles

Alan Arroyo¹ | Dan McQuillan² | R. Bruce Richter¹  | Gelasio Salazar³

¹Department of Combinatorics & Optimization, University of Waterloo, Waterloo, Ontario, Canada

²Department of Mathematics, Norwich University, Northfield, Vermont, USA

³Instituto de Física, Universidad Autónoma de San Luis Potosí, San Luis Potosí, Mexico

Correspondence

R. Bruce Richter, University of Waterloo
Email: brichter@uwaterloo.ca

Contract grant sponsor: CONACYT; contract grant sponsor: NSERC.

Abstract

There are three main thrusts to this article: a new proof of Levi's Enlargement Lemma for pseudoline arrangements in the real projective plane; a new characterization of pseudolinear drawings of the complete graph; and proofs that pseudolinear and convex drawings of K_n have $n^2 + O(n \log n)$ and $O(n^2)$, respectively, empty triangles. All the arguments are elementary, algorithmic, and self-contained.

KEYWORDS

empty triangles, Levi's Enlargement Lemma, pseudolinear drawing

AMS SUBJECT CLASSIFICATION

Primary 52C30, Secondary 05C10, 68R10

1 | INTRODUCTION

The Harary–Hill Conjecture asserts that the crossing number of the complete graph K_n is equal to

$$H(n) := \frac{1}{4} \left\lfloor \frac{n}{2} \right\rfloor \left\lfloor \frac{n-1}{2} \right\rfloor \left\lfloor \frac{n-2}{2} \right\rfloor \left\lfloor \frac{n-3}{2} \right\rfloor.$$

The work of Ábrego et al. [2] verifies this conjecture for “shellable” drawings of K_n ; this is one of the first works that identifies a topological, as opposed to geometric, criterion for a drawing to have at least $H(n)$ crossings.

Throughout this work, all drawings of graphs are *good drawings*: no two edges incident with a common vertex cross; no three edges cross at a common point; and no two edges cross each other more than once.

It is well-known that the *rectilinear* crossing number (all edges are required to be straight-line segments) of K_n is, for $n \geq 10$, strictly larger than $H(n)$. In fact, this applies to the more general *pseudolinear* crossing number.

The complexity of computing the cylindrical and the t -circle crossing number of a graph

Frank Duque

Instituto de Matemáticas
Universidad de Antioquia
Medellín, Colombia 050010

rodrigo.duque@udea.edu.co

Hernán González-Aguilar César Hernández-Vélez*

Facultad de Ciencias
Universidad Autónoma de San Luis Potosí
San Luis Potosí, México 78290

hernan@fc.uaslp.mx

cesar.velez@uaslp.mx

Jesús Leños[†]

Unidad Académica de Matemáticas
Universidad Autónoma de Zacatecas
Zacatecas, México 9800

jleanos@matematicas.reduaz.mx

Carolina Medina[‡]

Instituto de Física
Universidad Autónoma de San Luis Potosí
San Luis Potosí, México 78290

cmedina@ifisica.uaslp.mx

Submitted: Aug 2, 2017; Accepted: May 26, 2018; Published: Jun 8, 2018

© The authors. Released under the CC BY-ND license (International 4.0).

Abstract

A plane drawing of a graph is *cylindrical* if there exist two concentric circles that contain all the vertices of the graph, and no edge intersects (other than at its endpoints) any of these circles. The *cylindrical crossing number* of a graph G is the minimum number of crossings in a cylindrical drawing of G . In his influential survey on the variants of the definition of the crossing number of a graph, Schaefer lists the complexity of computing the cylindrical crossing number of a graph as an open question. In this paper, we prove that the problem of deciding whether a given graph admits a cylindrical embedding is NP-complete, and as a consequence we show that the t -cylindrical crossing number problem is also NP-complete. Moreover, we show

*Partially supported by FAPESP (Proc. 2013/03447-6) and CNPq (Proc. 456792/2014-7)

[†]Partially supported by CONACyT Grant 179867

[‡]Partially supported by CONACyT Grant 222667

Research Article

Dynamic Infrared Thermography of Nanoheaters Embedded in Skin-Equivalent Phantoms

K. A. López-Varela ¹, N. Cayetano-Castro,² E. S. Kolosovas-Machuca,³ F. J. González ³,
F. S. Chiwo,³ and J. L. Rodríguez-López ¹

¹*División de Materiales Avanzados, Instituto Potosino de Investigación Científica y Tecnológica, A.C., Camino Presa San José 2055, Lomas 4ª Secc., 78216 San Luis Potosí, SLP, Mexico*

²*Nanoscience, Micro and Nanotechnology Center, National Polytechnic Institute, Av. Luis Enrique Erro s/n, Zacatenco, 07738 Mexico City, Mexico*

³*Coordinación para la Innovación y la Aplicación de la Ciencia y la Tecnología, Universidad Autónoma de San Luis Potosí, San Luis Potosí, SLP, Mexico*

Correspondence should be addressed to K. A. López-Varela; karla.lopez@ipicyt.edu.mx and J. L. Rodríguez-López; jlrdez@ipicyt.edu.mx

Received 13 July 2017; Revised 1 November 2017; Accepted 5 December 2017; Published 14 January 2018

Academic Editor: Leszek A. Dobrzański

Copyright © 2018 K. A. López-Varela et al. This is an open access article distributed under the Creative Commons Attribution License, which permits unrestricted use, distribution, and reproduction in any medium, provided the original work is properly cited.

Nanoheaters are promising tools for localized photothermal therapy (PTT) of malignant cells. The anisotropic AuNPs present tunable surface plasmon resonances (SPR) with ideal NIR optical response to be applied as theranostic agents. To this purpose, nanoparticles with branches are suitable because of the electromagnetic field concentrated at their vertices. We standardized a protocol to synthesize multibranch gold nanoparticles (MB-AuNPs) by the seed-growth method and found a size-seed dependence tunability on the hierarchy of branching. Once the optical response is evaluated, we tested the temporal stability as nanoheaters of the MB-AuNPs immersed in skin-equivalent phantoms by dynamic infrared thermography (DIRT). The most suited sample presents a concentration of 5.2×10^8 MB-AuNPs/mL showing good thermal stability with $\Delta T = 4.5^\circ\text{C}$, during 3 cycles of 10 min at 785 nm laser irradiation with power of 0.15 W. According to these results, the MB-AuNPs are suitable nanoheaters to be tested for PTT in more complex models.

1. Introduction

The last twenty years' research reports on nanostructured materials clearly indicate their potential to develop new technologies for different specialized areas. The extensive investigation work in shape controlled synthesis of metal nanoparticles (NPs) has allowed the achievement of structures with complicated geometric forms and the use of nontoxic chemicals for their synthesis. Gold plays a particular and special role in this area of size and shape controlled synthesis, and because of their properties, those NPs are studied for technological applications in fields such as renewable energies, catalysis, medicine, and photonics. Because of the optical and low-reactive properties of gold nanoparticles (AuNPs), they

have been considered for medical applications as theranostic agents, which means that they can be simultaneously used for drug delivery [1], medical imaging [2–5], localized photothermal therapy (PTT) [6], and biological sensing [7, 8].

Nowadays, for some specific theranostic applications AuNPs are designed with anisotropic shapes, characteristic that tunes their surface plasmon resonance (SPR) from the visible to the near (NIR) and middle infrared (Mid-IR) regions of the spectra, also presenting local concentration of electromagnetic fields on the vertices [9]. The most common anisotropic AuNPs studied and used have been the gold nanorods (AuNRs) and stellated or spiky AuNPs, here termed multibranch gold nanoparticles (MB-AuNPs). The fact that NIR absorbance of MB-AuNPs fits the so-called therapeutic



Use of hafnium(IV) oxide in biosensors

Luis Carlos Ortiz-Dosal ^a, Gabriela Ángeles-Robles ^b,
and Eleazar Samuel Kolosovas-Machuca ^c

^aDoctorado Institucional en Ingeniería y Ciencia de Materiales (DICIM-UASLP), Universidad Autónoma de San Luis Potosí, San Luis Potosí, México; ^bPosgrado en Ciencias Interdisciplinarias, Instituto de Física, Universidad Autónoma de San Luis Potosí, San Luis Potosí, México; ^cCoordinación para la Innovación y Aplicación de la Ciencia y la Tecnología, Universidad Autónoma de San Luis Potosí, San Luis Potosí, México

ABSTRACT

Hafnium(IV) oxide is a material with properties that can increase the sensitivity, durability, and reliability of biosensors made from silicon dioxide and other semiconductor materials due to its high dielectric constant, thermodynamic stability, and the simplicity with which it can be deposited. This work describes the use of this material in biosensors based on field-effect transistors to detect ions and DNA, in immunosensors to detect an antigen-antibody complex, its use as a contrast material in computed tomography scans and the possibility of using it in optic biosensors in the infrared region. Its low cost and versatility in the field of biosensors is underscored.

KEYWORDS

Biosensor; immunosensor;
hafnium(IV) oxide; field-
effect transistor; DNA sensor

Introduction

Hafnium(IV) oxide (HfO_2) or hafnia has been studied extensively because its properties make it suitable for a variety of applications. In the form of thin films this material has a relatively high refraction index (1.89), a density of 9.7 g/cm^3 , and a high mechanical thermal (fusion point = 3031.15 K) and chemical stability. This stability is partially due the relatively high transition temperatures between its three crystalline phases, monoclinic, tetragonal, and cubic. It also has the advantage of being able to be deposited with different growth methods such as ultrasonic spray pyrolysis^[1], sol-gel^[2], sputtering^[3], atomic layer deposition^[4], and electron beam evaporation.^[5]

This material has the potential to be used as an electrical insulator in electronic and opto-electronic devices, due to its high dielectric constant, $\epsilon = 25$, which is four to six times greater than the dielectric constant of silicon dioxide^[6]; as well as having a higher band gap (5.3–5.9 eV), which makes it transparent to visible light. Therefore, this oxide is substituting silicon dioxide as insulator for the dielectric gates of metal-oxide-

CONTACT Luis Carlos Ortiz-Dosal carlos.ortiz@alumnos.uaslp.edu.mx Doctorado Institucional en Ingeniería y Ciencia de Materiales (DICIM-UASLP), Universidad Autónoma de San Luis Potosí, Av. Álvaro Obregón 64, San Luis Potosí, S.L.P. 78000, México

Color versions of one or more of the figures in the article can be found online at www.tandfonline.com/ljii.

RESEARCH ARTICLE

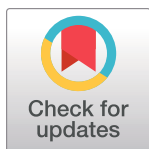
Development and validation of an algorithm to predict the treatment modality of burn wounds using thermographic scans: Prospective cohort study

Mario Aurelio Martínez-Jiménez^{1,2,3}, Jose Luis Ramirez-GarciaLuna^{1,4}*, Eleazar Samuel Kolosovas-Machuca⁵, Justin Drager⁴, Francisco Javier González⁵

1 Department of Surgery, Faculty of Medicine, Universidad Autónoma de San Luis Potosí, San Luis Potosí, SLP, Mexico, **2** Burn Unit, Hospital Central Dr. Ignacio Morones Prieto, San Luis Potosí, SLP, Mexico, **3** Doctorado Institucional en Ingeniería y Ciencia de Materiales (DICIM-UASLP), Universidad Autónoma de San Luis Potosí, San Luis Potosí, SLP, Mexico, **4** Division of Experimental Surgery, Faculty of Medicine, McGill University, Montreal, QC, Canada, **5** Coordinación para la Innovación y Aplicación de la Ciencia y la Tecnología, Universidad Autónoma San Luis Potosí, San Luis Potosí, SLP, Mexico

* These authors contributed equally to this work.

* jose.ramirezgarcialuna@mail.mcgill.ca



OPEN ACCESS

Citation: Martínez-Jiménez MA, Ramirez-GarciaLuna JL, Kolosovas-Machuca ES, Drager J, González FJ (2018) Development and validation of an algorithm to predict the treatment modality of burn wounds using thermographic scans: Prospective cohort study. PLoS ONE 13(11): e0206477. <https://doi.org/10.1371/journal.pone.0206477>

Editor: David M. Burmeister, US Army Institute of Surgical Research, UNITED STATES

Received: July 9, 2018

Accepted: October 12, 2018

Published: November 14, 2018

Copyright: © 2018 Martínez-Jiménez et al. This is an open access article distributed under the terms of the [Creative Commons Attribution License](https://creativecommons.org/licenses/by/4.0/), which permits unrestricted use, distribution, and reproduction in any medium, provided the original author and source are credited.

Data Availability Statement: All relevant data are within the paper and its Supporting Information files.

Funding: The authors received no specific funding for this work. JLRGL receives doctoral support from the Mexican National Council for Science and Technology (CONACYT) (<https://www.conacyt.gob.mx/>) and the Fonds de Recherche en Santé Québec (FRSQ) (www.frsq.gouv.qc.ca/en/). The funding

Abstract

Background

The clinical evaluation of a burn wound alone may not be adequate to predict the severity of the injury nor to guide clinical decision making. Infrared thermography provides information about soft tissue viability and has previously been used to assess burn depth. The objective of this study was to determine if temperature differences in burns assessed by infrared thermography could be used predict the treatment modality of either healing by re-epithelization, requiring skin grafts, or requiring amputations, and to validate the clinical predication algorithm in an independent cohort.

Methods and findings

Temperature difference (ΔT) between injured and healthy skin were recorded within the first three days after injury in previously healthy burn patients. After discharge, the treatment modality was categorized as re-epithelization, skin graft or amputation. Potential confounding factors were assessed through multiple linear regression models, and a prediction algorithm based on the ΔT was developed using a predictive model using a recursive partitioning Random Forest machine learning algorithm. Finally, the prediction accuracy of the algorithm was compared in the development cohort and an independent validation cohort. Significant differences were found in the ΔT between treatment modality groups. The developed algorithm correctly predicts into which treatment category the patient will fall with 85.35% accuracy. Agreement between predicted and actual treatment for both cohorts was weighted kappa 90%.



Antimycotic activity of zinc oxide decorated with silver nanoparticles against *Trichophyton mentagrophytes*

Rosalba Patiño-Herrera^{a,b,*}, R. Catarino-Centeno^c, Marissa Robles-Martínez^b,
María Guadalupe Moctezuma Zarate^d, J.C. Flores-Arriaga^b, Elías Pérez^{b,e}

^a Departamento de Ingeniería Química, Instituto Tecnológico de Celaya, Tecnológico Nacional de México, Av. Tecnológico y Antonio García Cubas s/n. Celaya, Guanajuato 38010, Mexico

^b Doctorado en Ingeniería y Ciencia de Materiales de la UASLP, Sierra Leona 530, San Luis Potosí, S.L.P. 78210, Mexico

^c Facultad de Ciencias, UASLP, Álvaro Obregón 64, San Luis Potosí S.L.P. 78000, Mexico

^d Facultad de Ciencias Químicas, UASLP, Álvaro Obregón 64, San Luis Potosí S.L.P. 78000, Mexico

^e Instituto de Física, UASLP, Álvaro Obregón 64, San Luis Potosí S.L.P. 78000, Mexico

ARTICLE INFO

Article history:

Received 14 January 2017

Received in revised form 10 October 2017

Accepted 1 January 2018

Available online 5 January 2018

Keywords:

ZnO-AgNPs

Antimycotic activity

Trichophyton mentagrophytes

Biofilm

Hydrophobic systems

ABSTRACT

Antimycotic behavior of zinc oxide decorated with silver nanoparticles (ZnO-AgNPs) against *Trichophyton mentagrophytes* (*T. mentagrophytes*) was investigated on this work. Silver decoration size was modulated during Ag₂O and Ag⁰ synthesis in aqueous solution at pH 11, 12 and 14, obtaining the smallest size at pH 12 and the largest at pH 14. In *ex-situ* tests, ZnO-AgNPs prevents successfully the growth of *T. mentagrophytes*, the percent mycelial inhibition (PMI) of formula F12 was 91.76% while formulas F12 and F14 was 100%, they also not present toxicity in cell viability, even the formula F12 promoted cell growth. Additionally, once *T. mentagrophytes* has grown it turns in a hydrophobic biofilm, whose water contact angle (WCA) was $127 \pm 3^\circ$, showing that no aqueous solution will have antimycotic activity against *T. mentagrophytes* biofilm. It has been propose a ZnO-AgNPs suspension in a hydrophobic fluid (polydimethylsiloxane, PDMS) that allowed to the particles permeate and permitted a direct contact with the biofilm, which was eliminated successfully. These results suggest that ZnO-AgNPs in a hydrophobic fluid emerge as a viable alternative for fungal infections treatment.

© 2018 Elsevier B.V. All rights reserved.

1. Introduction

Onychomycosis is the most often human nails disease, being responsible for more than half of nail disorder (onychodystrophy) cases. Typically it is a nail infection caused by fungus [1]. The injury affects toenail mainly and can be preceded and/or accompanied by an adjacent skin fungal infection [2]. This disease affects people of all ages, although it is rare in children. Onychomycosis can be acquired by users of swimming pools, gyms, spas, locker rooms, communal showers and other public places where moisture and walk barefoot favor transmission. Once infection begins, the nail commences to deform and with the passing of time turns on a dark brown and a thickness out of the ordinary, with the risk of breaking on or cause some bulge [3]. Onychomycosis is rarely life-threatening however, its high prevalence and associated morbidity make it a health public problem [4]. Nail infection caused by onychomycosis is a very common disease; previous studies reports prevalence rates between 2 and 18% of the population [5]. Background to this

disease are: immunosuppressive, poor peripheral circulation, diabetes, family history, age, occupation, social class, climate, living conditions, and skin disorders as hyperhidrosis, onychogryphosis and trauma nail [1,3]. Onychomycosis is caused by dermatophytes, yeasts, molds and non-dermatophytes. *Trichophyton*, *Microsporum* and *Epidermophyton* are responsible for almost 90% of nail onychomycosis and at least 50% of nail infections; from them, *Trichophyton rubrum* and *Trichophyton mentagrophytes* are the most common species of nail infection [6]. Topical treatment is not effective as oral therapy, both are associated with high rates of treatment failure and relapse [7], this may be due to unsuitable penetration through the nail keratin. Currently, oral terbinafine is the first-line treatment of onychomycosis; it has a clinical cure rate of 60% and a recurrence rate of 20% to 50% [7]. Alternate azole antifungals (itraconazole and fluconazole) as well griseofulvin has even lower clinical cure rates. The treatment of onychomycosis may take an antifungal therapy for a long time, usually 12 weeks of oral administration, which have side effects and interactions with other clinical medication. In addition, this treatment can be expensive [1]. Finally, disease relapses are common, especially in toenail onychomycosis. Patients whose treatment failures were never frees of diseases and infections for decades. Onychomycosis, from a medical point of view, is considered a cosmetic problem that does not require treatment; however, onychomycosis is

* Corresponding author at: Departamento de Ingeniería Química, Instituto Tecnológico de Celaya, Tecnológico Nacional de México, Av. Tecnológico y Antonio García Cubas s/n. Celaya, Guanajuato 38010, Mexico.

E-mail address: roos_ph@iqcelaya.itc.mx (R. Patiño-Herrera).



Friction coefficient between a hydrophobic soft solid surface and a fluid: Determined by QCM-D

Rosalba Patiño-Herrera^{a,b,*}, R. Catarino-Centeno^c, Armando Gama Goicochea^d,
Marissa Robles-Martínez^b, Ramiro Rico Martínez^a, Elías Pérez^e

^a Departamento de Ingeniería Química, Instituto Tecnológico de Celaya, Tecnológico Nacional de México, Av. Tecnológico y Antonio García Cubas s/n. Celaya, Guanajuato 38010, Mexico

^b Doctorado en Ingeniería y Ciencia de Materiales de la UASLP, Sierra Leona 530, San Luis Potosí 78210, Mexico

^c División de Ingeniería Mecatrónica, Instituto Tecnológico Superior de Zacapoaxtla, Zacapoaxtla 73680, Puebla, Mexico

^d División de Ingeniería Química y Bioquímica, Tecnológico de Estudios Superiores de Ecatepec, Avenida Tecnológico s/n, Ecatepec de Morelos 55210, Estado de México, Mexico

^e Instituto de Física, UASLP, Álvaro Obregón 64, San Luis Potosí 78000, Mexico

ARTICLE INFO

Keywords:

QCM-D
Friction coefficient
Hydrophobic film
Highly concentrated solutions
Lubricant

ABSTRACT

Quartz crystal microbalance with dissipation (QCM-D) response data was used to determine the friction coefficient (μ) between soft solid surface and ethanol. A self-assembly of Dodecanethiol (DCT) film on gold was carried out. The number of DCT grafted (T) onto gold surface was investigated at concentrated solutions (10–33% v/v). Such large concentration leads to an increase on grafting density, viscosity, roughness and water contact angle favoring the reduction of friction coefficient (~ 0.0922). These results allow proposing a soft self-assembled hydrophobic film to reduce friction between fluids into conduit, tube, or some other device.

1. Introduction

When a fluid flows through a conduit, tube, or some other device, energy loss occurs due to friction between liquid and pipe wall as result of the decrease in pressure between two points in the flow system. In long structures, friction losses are very important and have been the subject of experimental and theoretical studies. In this way the energy will decrease in movement direction due to the resistance that surface in contact with fluid will offer to the movement of it. Reduction of friction at solid/liquid interface is important to energy efficiency; for example, total frictional losses in a typical diesel engine exceed 10% of total combustion energy. Therefore, today lubrication technologies are focused on wear elimination over frictional energy losses [1]. All surfaces contain small asperities and irregularities (rough and uneven surfaces), regardless of how fine they are polished, it impact friction on the surface. The main challenge is to reduce the friction and therefore the friction coefficient as much as possible, either by removing the factors that may have an adverse effect on the surfaces in relative movement or by controlling these factors. Some factors that affect the friction coefficient are temperature, operating load, speed between the surfaces, type of lubricant and surface roughness. A technique to reduce the friction coefficient is by adsorbing nano-organic films that have a

high percentage of their atoms on the surface. Hence, physical properties of nanostructures depend to a much greater extent on their surface and interfacial environment [2].

In this work, the main motivation was grafting a variety of molecules on the surface by modifying of self-assembled to produce structured films. Modification of noble metals with self-assembles molecules is particularly important due to simplicity of preparation, versatility, stability, adaptability, high adsorbing density, reproducibility, ordered structure, and the possibility of introducing different chemical functionalities [3,4]. Among the alkanethiols, dodecanethiol (DCT) adsorbed on gold is considered to be prototypical for the surface modification and SAMs formation [5]. Interfacial phenomena on SAMs are directly related to corrosion [6,7], adhesion [6,8], charge transfer through molecules [9], electrochemical barriers [2], nucleation and growth of crystals on surfaces [10], model surfaces for biochemistry and cell biology [11] and wetting [6,12].

The aim was to characterize the interactions between a hydrophobic soft solid surface and a fluid (ethanol) to identify those terms that make the soft solid surface a good boundary lubricant. The response data of quartz crystal microbalance with dissipation provides information to calculate the number of grafted molecules, normal forces, friction forces and friction coefficient between soft solid film and a fluid,

* Corresponding author at: Departamento de Ingeniería Química, Instituto Tecnológico de Celaya, Tecnológico Nacional de México, Av. Tecnológico y Antonio García Cubas s/n. Celaya, Guanajuato 38010, Mexico.

E-mail address: roos_ph@iqcelaya.itc.mx (R. Patiño-Herrera).

<https://doi.org/10.1016/j.chemphys.2018.06.023>

Received 13 April 2017; Accepted 28 June 2018

Available online 30 June 2018

0301-0104/ © 2018 Elsevier B.V. All rights reserved.



Review

Morphological changes in erythrocytes of people with type 2 diabetes mellitus evaluated with atomic force microscopy: A brief review



Alejandra Loyola-Leyva^a, Juan Pablo Loyola-Rodríguez^{b,*}, Marco Atzori^c,
Francisco Javier González^d

^a Basic Biomedical Sciences Doctoral Program, Faculty of Medicine, San Luis Potosí Autonomous University, Avenida Venustiano Carranza 2405, Los Filtrros, 78210, San Luis, S.L.P., Mexico

^b Faculty of Dentistry, Baja California Autonomous University, Blvd. Univesitario 1000, Unidad Valle de las Palmas, Tijuana, Baja California, Mexico

^c Faculty of Sciences, San Luis Potosí Autonomous University, Lateral Av. Salvador Nava, Lomas, 78290, San Luis, S.L.P., Mexico

^d Innovation and Application of Science and Technology Center (CIACyT), San Luis Potosí Autonomous University, Avenida Sierra Leona 550, Lomas 2ª sección, 78210, San Luis, S.L.P., Mexico

ARTICLE INFO

Keywords:

Erythrocytes
Morphology
Type 2 diabetes mellitus
Atomic force microscopy
Cardiovascular diseases

ABSTRACT

Prevalence of type 2 diabetes mellitus (T2DM) has been increasing worldwide. Cardiovascular diseases are one of the main causes of death among people with T2DM. Morphological changes in erythrocytes have been associated with higher risk of cardiovascular diseases. Atomic force microscopy (AFM) is a new technique that allows non-invasive imaging of cells and the evaluation of changes in mechanical properties.

Aim: To evaluate by AFM the erythrocytes morphological changes of people with T2DM

Methods: Search was conducted from in PubMed, ScienceDirect, Scielo, and Lilacs. Erythrocyte, type 2 Diabetes Mellitus and, Microscopy, Atomic Force were the keywords used for the search. Papers included were cross-sectional studies performed in humans.

Results: Five of seven articles fulfilled the inclusion criteria. Compared with healthy cells, the erythrocytes from individuals affected by T2DM had morphological changes such as a decreased concave depth, diameter, height and a deformation index, while axial ratio, stiffness, adhesive force, aggregation, and rigidity index were increased. The results regarding the erythrocyte roughness were inconclusive.

Conclusions: The AFM is an excellent instrument to study the altered erythrocytes of subjects affected by T2DM. Morphology changes in erythrocytes could lead to cardiovascular events, which are major complications in people living with this disease

1. Introduction

Diabetes is one of the largest health emergencies of the 21st century. Type 2 diabetes mellitus (T2DM) is the most common condition, and its prevalence has been increasing worldwide in the last few decades. Moreover, it is estimated by 2030 there will be 552 millions of people affected by this disease. Besides, cardiovascular disease is one of the leading causes of death among subjects affected by T2DM and could account for 50% or more of the deaths (International Diabetes Federation, 2015).

Morphology changes in the structure, shape, and function of the erythrocytes, as well as some rheological changes such as decreased deformability and increased aggregation have been associated with

higher risk of cardiovascular diseases (Diez-Silva et al., 2010; Soma and Pretorius, 2015). Erythrocytes are biconcave cells, without a nucleus or mitochondria and take part in the inflammatory response. Its membrane comprises two domains, an overlaying asymmetric phospholipid bilayer membrane and an underlying spectrin-actin cytoskeletal interconnected by junctional complexes (Almqvist et al., 1994; Liu et al., 2003). Some of these abnormalities in individuals with diabetes are caused by the reduction in the cholesterol to phospholipid ratio in the lipid bilayer of the erythrocyte membrane (Soma and Pretorius, 2015). Also, there is an enhanced fibrinogen production by insulin, which contributes to hyperfibrinogenemia and therefore to an increased cardiovascular risk through aggregation of erythrocytes (Barazzoni et al., 2003).

Abbreviations: T2DM, type 2 diabetes mellitus; AFM, atomic force microscopy; STROBE, strengthening the reporting of observational studies in epidemiology; SEM, scanning electron microscopy

* Corresponding author.

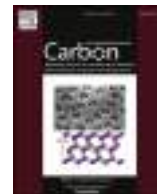
E-mail addresses: aleloleyva@yahoo.com.mx (A. Loyola-Leyva), juanpablo.loyola8@gmail.com (J.P. Loyola-Rodríguez), marco_atzori@hotmail.com (M. Atzori), javier.gonzalez@uaslp.mx (F.J. González).

<https://doi.org/10.1016/j.micron.2017.11.001>

Received 18 September 2017; Received in revised form 1 November 2017; Accepted 2 November 2017

Available online 10 November 2017

0968-4328/ © 2017 Elsevier Ltd. All rights reserved.



Synthesis of carbon nano-onions doped with nitrogen using spray pyrolysis

E. Tovar-Martinez^{a, b}, J.A. Moreno-Torres^b, J.V. Cabrera-Salazar^a, M. Reyes-Reyes^b, Luis F. Chazaro-Ruiz^c, R. López-Sandoval^{a, *}

^a Advanced Materials Department, IPICYT, Camino a La Presa San José 2055, Col. Lomas 4a Sección, San Luis Potosí, 78216, Mexico

^b Instituto de Investigación en Comunicación Óptica, Universidad Autónoma de San Luis Potosí, Álvaro Obregón 64, San Luis Potosí, 78000, Mexico

^c Environmental Science Department, IPICYT, Camino a La Presa San José 2055, Col. Lomas 4a Sección, San Luis Potosí, 78216, Mexico

ARTICLE INFO

Article history:

Received 12 June 2018

Received in revised form

21 August 2018

Accepted 27 August 2018

Available online 28 August 2018

ABSTRACT

In this work, we have synthesized carbon nano-onions (CNOs) doped with nitrogen and iron carbide core. These nanostructures were synthesized pyrolysing various alcohol-benzylamine reaction mixtures. These CNOs showed a certain degree of functionalization of their surfaces, depending of the solvent, as well as *n*-type doping due to the inclusion of N atoms in the graphene layers. Ratios of O atoms to C atoms as well as to N atoms of the pyrolyzed solution play an important role in the morphology of the CNOs and on the phase of the iron core. Differences in the morphology of the samples have an important effect on their electrical conductivity as well as in their electrochemical properties. Synthesized samples showing well-defined CNOs, the sintering between them is negligible, have a low conductivity and higher capacitance, while those samples showing the best conductivities and lower capacitances, the CNOs in samples are connected between them by turbostratic graphite ribbons, in similar way to the CNOs synthesized from carbon nanodiamond annealed in argon atmosphere.

© 2018 Elsevier Ltd. All rights reserved.

1. Introduction

Nanoparticles can be protected from degradation due to environmental conditions, at the same time that their intrinsic properties are preserved when they are encapsulated. Some of the structures that encapsulate are carbon nanotubes or carbon layers [1,2]. The encapsulation of nanoparticles has attracted the attention for its promising applications, such as in information technology and biomedicine [3–6]. In some technological applications, such as in gas sensors, it is possible to use hollow carbon nanoparticles instead of carbon layers encapsulating nanoparticles [7,8]. In other cases, these carbon nanoparticles are quasi-spherical and consist only of concentric graphene layers [9–11]. In general, these kind of carbon are indistinctly called carbon nano-onions (CNOs) [11]. CNOs were discovered by S. Iijima in 1980 [9], but it was D. Ugarte who reported a reproducible technique for obtaining these nanostructures by irradiation of carbon soot with an electron beam [10]. Several techniques have been used for the synthesis of this material

[11]. However, the most widely used method is the graphitization of carbon nanodiamonds at high temperatures (1100–1700 °C) in an inert gas or under vacuum conditions [11–14]. Other techniques to synthesize CNOs include laser excitation, ion implantation and chemical vapor deposition (CVD) [15–20].

CNOs have good electrical characteristics for their use in electrical double layer capacitors (EDLC) because they can be synthesized with small diameters <10 nm [21–24], which make them suitable for their use in EDLC. This is related to the fact that the smaller the CNOs diameters, the larger the exposed surface area and, thus, much larger the capacitance [11,21–24]. However, the use of CNOs in EDLC, as well as in other possible technological applications, requires their surface functionalization [25–27] and, in some cases, the modification of their electronic properties [28–30]. In general, the surface functionalization of CNOs is carried out by chemical oxidation either with inorganic acids [31,32] or with potassium hydroxide [33]. This chemical activation generates surface oxygenated functional groups, which increase the solubility of the CNOs in polar solvents. However, this surface functionalization generates defects and, as a consequence, a loss of the sp² character of the graphene layer, with a consequent loss of its great electrical conductivity. To retain the high conductivity of CNOs, it is

* Corresponding author.

E-mail address: sandov@ipicyt.edu.mx (R. López-Sandoval).

A Home-Made Trap Baited With Sex Pheromone for Monitoring *Spodoptera frugiperda* Males (Lepidoptera: Noctuidae) in Corn crops in Mexico

Edi A. Malo,^{1,3} Samuel Cruz-Esteban,¹ Francisco J. González,² and Julio C. Rojas¹

¹Departamento de Agricultura, Sociedad y Ambiente, Grupo de Ecología y Manejo de Artrópodos, El Colegio de la Frontera Sur (ECOSUR), Carretera Antiguo Aeropuerto km 2.5, CP 30700, Apartado Postal 36 C. P. 30700, Tapachula, Chiapas, Mexico,

²Coordinación para la Innovación y la Aplicación de la Ciencia y la Tecnología, Universidad Autónoma de San Luis Potosí, Sierra Leona 550, Lomas 2da. Sección, 78210 San Luis Potosí, SLP, Mexico, and ³Corresponding author, e-mail: emr@ecosur.mx

Subject Editor: Michael Brewer

Mention of commercial products in this publication is solely for the purpose of reporting research findings and does not imply a recommendation, endorsement, or discommendation by El Colegio de la Frontera Sur.

Received 24 January 2018; Editorial decision 22 April 2018

Abstract

Fall armyworm (FAW), *Spodoptera frugiperda* (J. E. Smith), populations are monitored with a variety of commercial sex pheromone-baited traps. However, a number of trap-related variables may affect the number of FAW males captured. In this study, we tested the effect of trap design, trap size, and trap color for monitoring FAW males in corn crops in Mexico. We found that plastic jug trap (a home-made trap), captured significantly more FAW males than a commercial trap (Scentry *Heliothis*) and water bottle trap (another home-made trap). We also found that size of plastic jug traps (3.78, 10, or 20 liters) did not affect the captures of FAW males. Our results indicated that plastic yellow jug traps captured significantly more males than blue and black traps. Plastic jug white, red, and green traps captured a similar number of FAW males than plastic jug yellow, blue, and black traps. Plastic jug blue, white, and yellow traps captured more nontarget insects compared to black traps. The number of nontarget insects captured by green and red traps was similar and not significantly different to that caught by blue, white, yellow, and black traps. Traps captured more individuals from Diptera than Coleoptera and Hymenoptera. Overall, the results suggest that yellow plastic jug may be used for monitoring FAW males in corn and sorghum crops in Mexico.

Key words: fall armyworm, corn, monitoring, pheromone, trap

Pheromones can be used in four strategies in integrated pest management programs, specifically monitoring, mass trapping, attraction–annihilation, and mating disruption (Howse et al. 1998). Trap variables, such as design, size, and color are important features, along with the attractant, in the first three strategies. Ideally, traps should be easy to use, of standard construction, and inexpensive (Wall 1990). When a trap is constructed, characteristics such its design, size, and color in relation to the insect behavior should be considered (Howse et al. 1998). A variety of traps have been designed for several insect pests and many of them are commercially available. However, a number of biological and environmental factors can affect traps efficiency and use in insect pest management programs. For example, delta sticky traps can become saturated if the populations of the target insect are very high. Additionally, sticky traps require more preparation and handling time in the field compared to nonsticky traps (Knodel and Agnello 1990). Trap color may influence the

number of target insects, including predators, parasitoids (Blackmer et al. 2008, Roubos and Liburd 2008), and pollinators (Knight and Miliczky 2003, Roubos and Liburd 2008). Attraction of beneficial insects to trap colors needs to be addressed during trap development in order to minimize nontarget effects.

Commercially available sex pheromone-baited traps have been used in a number of countries for monitoring the fall armyworm (FAW), *Spodoptera frugiperda* (J. E. Smith), males in corn fields (Adams et al. 1989, Mitchell et al. 1989, Gross and Carpenter 1991, Andrade et al. 2000, Malo et al. 2001, 2004). For example, in the United States, *S. frugiperda* males are frequently monitored with plastic funnel traps (e.g., Universal moth traps, bucket traps, or uni-traps) (Mitchell et al. 1985, Tumlinson et al. 1986). However, funnel traps had a poor efficiency compared to Scentry *Heliothis* and delta traps in catching FAW males in the coastal plain of Chiapas, Mexico (Malo et al. 2001). Scentry *Heliothis* trap was the most effective trap



Study of Polymer-Solvent Interactions of Complex Polysiloxanes Using Dissipative Particle Dynamics

Javier Vallejo-Montesinos^a, Antonio Villegas^a, Jorge Cervantes^a, Elías Pérez^b, and Armando Gama Goicochea^c

^aDivisión de Ciencias Naturales y Exactas, Universidad de Guanajuato, Guanajuato, Mexico; ^bInstituto de Física, Universidad Autónoma de San Luis Potosí, San Luis Potosí, Mexico; ^cDivisión de Ingeniería Química y Bioquímica, Tecnológico de Estudios Superiores de Ecatepec, Ecatepec, Mexico

ABSTRACT

The mesoscopic modeling of three polysiloxanes in solution is reported in this work, with the purpose of predicting their physico-chemical properties as functions of the quality of the solvent, so that a judicious choice of polymer/solvent can be made for various applications. The polymers studied were the following polysiloxanes: polydimethylsiloxane (PDMS), polysiloxane with a bulky alkyl side group (PMHS) and a siloxane copolymer with a hydrophilic polar side group (P2DMPAS). The model used and solved through numerical simulations is the one known as dissipative particle dynamics. Density profiles and radial distribution functions were calculated for each system. We analyzed how the polymers behave in the presence of solvents of varying quality and compared their behavior with experimental data. We observed that we could replicate the behavior in good solvents for PDMS and PMHS. We also observed in the simulation box the formation of pseudo-micelles for P2DMPAS.

KEYWORDS

Dissipative Particle Dynamics (DPD); Polydimethylsiloxane; Polymethylhexylsiloxane; solvent quality

Introduction

Polysiloxanes are materials with a wide range of applications, largely due to their desirable properties, such as high flexibility, thermal resistance, and exposure to UV light resistance, among others.^[1,2] Since they are often polymerized in and processed from solution, it is very important to understand their interactions and associations with diverse solvents. For these materials, multiple synthetic routes can be used,^[1,2] however, aside from polydimethylsiloxane, little has been reported regarding solution behavior for this family of polymers. Changing the side group in a polysiloxane can change its solubility in various solvents, or lead even to unusual behavior, as we have reported previously.^[3–6] For example, we reported earlier^[4] the analysis of the second virial coefficient, A_2 , for a series of polysiloxane chains with different side groups; the effect of the side group and molecular weight on the value of A_2 was analyzed through the Helical Worm (HW) chain type model.^[7] The theoretical analysis of the interpenetration



Research paper

Complexity functions for networks: Dynamical hubs and complexity clusters



Valentin Afraimovich^{a,b}, Aleksei Dmitrichev^{b,*}, Dmitry Shchapin^b,
Vladimir Nekorkin^b

^a Instituto de Investigacion en Comunicacion Optica, Universidad Autonoma de San Luis Potosi, Karakorum 1470, Lomas 4a, San Luis Potosi, SLP 78220, Mexico

^b Institute of Applied Physics RAS, 46 Ul'yanov Street, Nizhny Novgorod, 603950, Russia

ARTICLE INFO

Article history:

Received 23 March 2017

Revised 7 July 2017

Accepted 8 July 2017

Available online 10 July 2017

Keywords:

Dynamical network

Instability

Complexity

ABSTRACT

A method for studying the behavior of the elements of dynamical networks is introduced. We measure the amount of instability stored at each element according to the value of the mean complexity related to this element. Elements with close values of the mean complexity can be unified into complexity clusters; elements with the smallest values of complexities form dynamical hubs. The effectiveness of the method is manifested by its successive application to networks of coupled Lorenz systems.

© 2017 Elsevier B.V. All rights reserved.

1. Introduction

In the last years, scientists pay considerable attention to the study of complex networks, i.e., systems consisting of a large number of interacting subsystems (elements). Such systems can occur in physics, chemistry, biology, neuroscience, sociology, etc. Complex networks can be divided into two classes, namely, static and dynamical ones. In the static networks there is no individual dynamics at elements and couplings, and the geometry (topology) of coupling is fixed [1–4]. Therefore, the behavior of such networks is determined only by the geometry (topology) of coupling. On the other hand, in the dynamical ones either elements and/or the couplings and/or geometry (topology) of coupling can vary with time according to the dynamical law [5–7]. While a theory of static networks is now well developed, and, in particular, many different quantities (such as vertex degree, average distance, shortest path, clustering coefficient, etc) have been introduced and used, no general theory exists for dynamical networks (DN), and only a few characteristics reflecting the features of their dynamics were presented.

In this article, we restrict our study to the class of DN where the geometry of coupling is fixed, but each element possesses its own dynamics. We suggest a new characteristic for such a DN, which takes into account both the topology of its coupling and the individual dynamics of its elements. We deal with DN that (for the case of continuous time) is a system of the form

$$\dot{y} = F(y), y = \{y_i\}, y_i \in R^{p_i}, p := \sum p_i, \quad (1)$$

* Corresponding author.

E-mail addresses: valentin.afraimovich@gmail.com (V. Afraimovich), admitry@neuron.appl.sci-nnov.ru (A. Dmitrichev), vnekorkin@neuron.appl.sci-nnov.ru (V. Nekorkin).